EFDC+
General Ocean Turbulence Module
White Paper

October 18, 2023
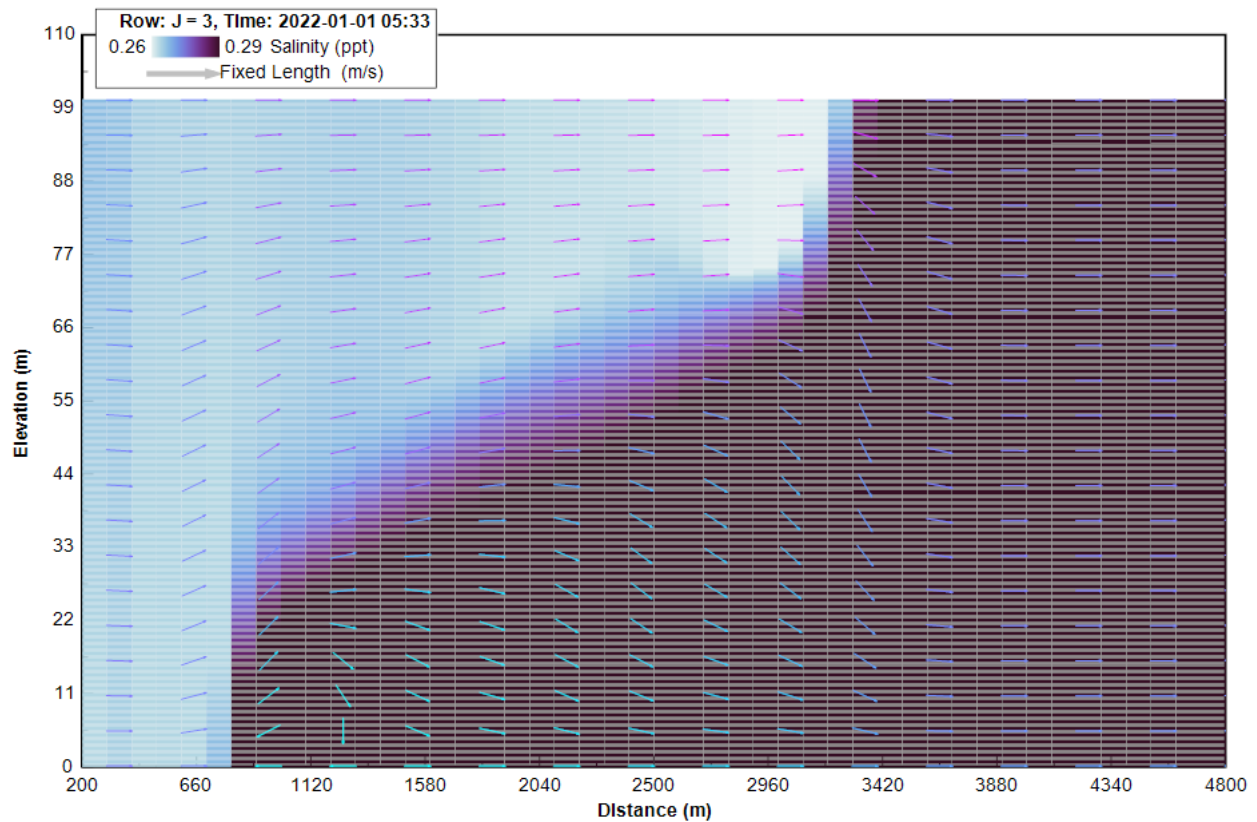
DSI, LLC
Edmonds, WA USA

This page left intentionally blank.

Abstract

The aim of this paper is to describe the coupling of the General Ocean Turbulence Model (GOTM) with the Environmental Fluid Dynamics Code Plus (EFDC+), which has been recently implemented. One of the key components of EFDC hydrodynamics is the approach for turbulence closure. Historically this has been limited to the famous Mellor-Yamada level-2.5 turbulence closure scheme, which uses various second-moment closure approaches. This approach has been largely unchanged for nearly 30 years, and the recent addition of various first- and second-order closure approaches by way of the coupling of EFDC+ with the GOTM subroutines represents the most significant addition to the hydrodynamic capabilities of EFDC to date.

GOTM is a one-dimensional water column model for the most important hydrodynamic and thermodynamic processes related to vertical mixing in natural waters. GOTM has been conceived as a library of turbulence models that can be readily interfaced with 3-D circulation models. It is a core component of other popular coastal and ocean models such as FVCOM, TELEMAC, and GETM. GOTM features an extensive list of turbulence options, and at least one member of every relevant model family can be found in GOTM, including empirical models, energy models, two-equation models, Algebraic Stress Models, and K-profile parameterizations.

This paper describes the theoretical basis of hydrodynamics in both EFDC and the GOTM Generic Length Scale approach, as well as the implementation of the coupling subroutines within EFDC+. In addition to the coupling of EFDC+ and GOTM, recent changes to the EFDC+ Explorer Hydrodynamics Module Interface have also been described. To improve the usability of the new turbulence closure options from GOTM, EFDC+ Explorer provides four new preset options as well as new graphical interfaces to allow for extensive customization of the turbulence closure options, and access to the wide array of features available in GOTM.

To verify and validate the coupling of EFDC+ and the GOTM turbulence subroutines, three test cases have been formulated and evaluated based on literature examples. These include an example of open channel flow, wind-induced currents in a closed basin, and free convection. In all test cases, analytical solutions have been compared to the predictions of various numerical turbulence closure models included with the updated version of EFDC+. To demonstrate the updated capabilities of the EFDC+ model for a real-world application, different closure approaches have been compared with observed conditions of thermal stratification in Lake Washington (King County, Washington). The results of these evaluations demonstrate that the coupling between EFDC+ and GOTM has been successfully implemented.

Contents

List of Figures

List of Tables

Chapter 1

Introduction

1.1. Background

1.1.1 EFDC+ Background

Environmental Fluid Dynamics Code Plus (EFDC+) is based on the public-domain, open-source version of EFDC originally developed at Virginia Institute of Marine Science (Hamrick 1992). It was designed to simulate three dimensional flow, transport, and biogeochemical processes in surface water systems (e.g., lakes, rivers, tributaries, marshes, wet and dry littoral margins, and coastal regions). Since the early development of EFDC, many new features and modules have been added and applied to a wide range of environmental studies including water quality, sediment transport, Lagrangian particle tracking, hydraulic structures, and chemical fate and transport.

EFDC uses a curvilinear-orthogonal grid with a sigma vertical coordinate system. The equations that form the basis of the EFDC hydrodynamic model are based on the continuity and hydrostatic, free-surface, Reynolds-averaged Navier–Stokes (RANS) equations. A two-equations turbulence-closure model developed by Mellor and Yamada (1982) and modified by Galperin et al. (1988) was implemented to simulate vertical turbulent viscosity and mass turbulent diffusivity in the model. Horizontal diffusion is calculated with the Smagorinsky (1963) formula.

1.1.2 GOTM Background

General Ocean Turbulence Model (GOTM) is an open-source of one-dimensional water column model for simulating hydrodynamic and thermodynamic processes related to vertical mixing in natural waters (Burchard, Bolding, and Villarreal 1999; Burchard and Bolding 2001; Umlauf and Burchard 2005). GOTM has been used in many studies, for example, the evolution of thermal stratification in the North Sea and the northern Pacific (Burchard and Bolding 2001), effects of breaking surface waves on surface boundary layer dynamics (Jones and Monismith 2008), mixing in sloping bottom boundary layers (Umlauf and Burchard 2011), and sediment dynamics, etc.

One of the primary strengths of the General Ocean Turbulence Model (GOTM) lies in its extensive

collection of well-tested turbulence models integrated within the code to facilitate the calculation of vertical turbulent fluxes. Its fashion contains a range of approaches, spanning from algebraic equations employed to compute turbulence kinetic energy (TKE) and turbulence length-scale to the utilization of two-equation models, in which both mentioned terms are computed from differential transport equations. The second-order model is an essential part of GOTM, with a full or approximate solution of the transport equations for the turbulent momentum fluxes. As an independent module, the turbulence module in GOTM has been integrated into several three-dimensional hydrodynamic models, including the General Estuarine Transport Model (GETM) (Burchard and Bolding 2002), the Regional Ocean Modelling System (ROMS) (Haidvogel et al. 2000), the Nucleus for European Modelling of the Ocean (NEMO) (Madec et al. 1991), the Finite Volume Community Ocean Model (FVCOM) (Chen et al. 2003).

For further information regarding the GOTM, readers should refer to the official GOTM website (https://www.gotm.net). The website provides access to the source code, comprehensive documentation, and various test scenarios, allowing for more detailed model exploration.

1.2. Objective

On that basis, the coupling of Environmental Fluid Dynamics Code Plus (EFDC+) and the General Ocean Turbulent Model (GOTM) has been implemented to add flexibility to the EFDC+ model by providing various turbulence models, including the $k - kl$, $k - \varepsilon$, $k - \omega$, and the generic length scale approaches, and to expand the capabilities for the description of vertical mixing processes. Users can choose one of the popular closures or define a new closure by specifying a few parameters. As a result, the effect of turbulence models on processes, such as sediment transport and eutrophication, can also be evaluated. Different options are available for K-Profiles Parameterization using the CVMix package (currently integrated with GOTM) and Langmuir turbulence and Stokes drift. These features offer enhanced capabilities, improved simulation accuracy, realism, and numerical stability, especially when simulating stratified systems in EFDC+.

Chapter 2

Theoretical Overview

In this chapter, we introduce a brief review of the primitive equations solved by EFDC, starting by the basic hydrodynamic equations, formulations of turbulence closures implemented in GOTM, and boundary conditions.

2.1. Basic Hydrodynamic Equations

The governing equations for water flows begins with the vertically hydrostatic boundary layer form of the turbulent equations of motion for an compressible, variable density fluid. Utilizing a time variable mapping transformation in the sigma coordinate system and the Boussinesq approximation for variable density results in the momentum and continuity equations and the transport equations for salinity in the following form:

The momentum equation in the x direction:

$$
\begin{aligned}
&\partial_t (mHu) + \partial_x (m_y Huu) + \partial_y (m_x Hvu) + \partial_z (mwu) - (mf + v\partial_x m_y - u\partial_y m_x) Hv \\
&= -m_y H \partial_x (g\zeta + p) - m_y (\partial_x h - z\partial_x H) \partial_z p + \partial_z (mH^{-1} A_V \partial_z u) + Q_u
\end{aligned}
\tag{2.1}
$$

The momentum equation in the y direction:

$$
\begin{aligned}
&\partial_t (mHv) + \partial_x (m_y Huv) + \partial_y (m_x Hvv) + \partial_z (mwu) + (mf + v\partial_x m_y - u\partial_y m_x) Hu \\
&= -m_x H \partial_y (g\zeta + p) - m_x (\partial_y h - z\partial_y H) \partial_z p + \partial_z (mH^{-1} A_V \partial_z v) + Q_v
\end{aligned}
\tag{2.2}
$$

The momentum equation in the z direction:

$$
\partial_z p = -gH (\rho - \rho_0) \rho_0^{-1} = -gHb
\tag{2.3}
$$

The continuity equations of both internal and external modes:

$$
\partial_t (m\zeta) + \partial_x (m_y Hu) + \partial_y (m_x Hv) + \partial_z (mw) = 0
\tag{2.4}
$$

$$
\partial_t (m\zeta) + \partial_x \left(m_y H \int_0^1 u\, dz \right) + \partial_y \left(m_x H \int_0^1 v\, dz \right) = 0
\tag{2.5}
$$

The equation of state:

$$\rho = \rho\,(p, S, T) \tag{2.6}$$

The transport equations for salinity and temperature:

$$\partial_t\,(mHS) + \partial_x\,(m_y HuS) + \partial_y\,(m_x HvS) + \partial_z\,(mwS) = \partial_z\left(mH^{-1}A_B\partial_z S\right) + Q_S \tag{2.7}$$

$$\partial_t\,(mHT) + \partial_x\,(m_y HuT) + \partial_y\,(m_x HvT) + \partial_z\,(mwT) = \partial_z\left(mH^{-1}A_B\partial_z T\right) + Q_T \tag{2.8}$$

In these equations, u and v are the horizontal velocity components in the curvilinear, orthogonal coordinates x and y, m_x and m_y are the square roots of the diagonal components of the metric tensor, $m = m_x m_y$ is the Jacobian or square root of the metric tensor determinant. The vertical velocity w is in the stretched, dimensionless vertical coordinate z. The total depth, $H = h + \zeta$ is the sum of the depth below and the free surface displacement. The pressure p is the physical pressure in excess of the reference density ρ_0 hydrostatic pressure, which defines the buoyancy b. In the momentum equations (2.1, 2.2), f is the Coriolis parameter, A_V is the vertical turbulent viscosity, and Q_u and Q_v are momentum source-sink terms. In the transport equations for salinity S and temperature T (2.7, 2.8), A_B is the vertical turbulent diffusivity, Q_S and Q_T are the source and sink terms.

The equations (2.1 - 2.8) provides a system of equations for variables u, v, w, p, ζ, ρ, S and T. The turbulent viscosity and diffusivity need to be specified to close this system of equations, together with the source and sink terms. In the original EFDC+, the second-moment turbulence closure model developed by Mellor and Yamada (1982) is used to compute the turbulent viscosity and diffusivity. The next section reviews the popular two-equation turbulence closure models implemented in GOTM.

2.2.   Turbulence models in GOTM

2.2.1   The Generic Length-Scale Model

For brevity, we present the generic length-scale (GLS) approach to two-equation turbulence models implemented in GOTM, which provides a general framework to recover many of the popular two-equation turbulence models as described in Umlauf and Burchard (2003). The first equation in the GLS model is the standard equation for transport of the turbulent kinetic energy k, while the second equation describes the transport of a generic parameter ψ, used to establish the turbulence length-scale quantity l. The first equation is:

$$\frac{\partial k}{\partial t} + u\frac{\partial k}{\partial x} + v\frac{\partial k}{\partial y} + w\frac{\partial k}{\partial z} = \frac{\partial k}{\partial z}\left(\frac{A_V}{\sigma_k^{\psi}}\frac{\partial k}{\partial z}\right) + P + B - \varepsilon \tag{2.9}$$

where σ_k^{ψ} is the turbulence Schmidt number for k, and ε is the rate of dissipation of k. The terms P and B represent production by shear and buoyancy as:

$$P = A_V \left[\left(\frac{\partial u}{\partial z}\right)^2 + \left(\frac{\partial v}{\partial z}\right)^2 \right] \tag{2.10}$$

$$B = A_B \frac{g}{\rho_0} \frac{\partial \rho}{\partial z} \tag{2.11}$$

The second equation in the GLS model is:

$$\frac{\partial \psi}{\partial t} + u\frac{\partial \psi}{\partial x} + v\frac{\partial \psi}{\partial y} + w\frac{\partial \psi}{\partial z} = \frac{\partial \psi}{\partial z}\left(\frac{A_v}{\sigma_\psi}\frac{\partial \psi}{\partial z}\right) + \frac{\psi}{k}\left(c_{\psi 1}P + c_{\psi 3}B - c_{\psi 2}\varepsilon F_{wall}\right) \tag{2.12}$$

where $c_{\psi 1}$, $c_{\psi 2}$ and $c_{\psi 3}$ are model constants to be determined based on experimental observations, the parameter σ_ψ is the turbulence Schmidt number for ψ. It is important to note that ψ must be uniquely related to the fields of k and l according to:

$$\psi = \left(c_\mu^0\right)^P k^m l^n \tag{2.13}$$

where c_μ^0 is the stability coefficient based on experimental data, and p, m, and n are coefficients unique to each particular turbulence scheme.

The dissipation rate, ε, then can be computed for any given pair of k and ψ as:

$$\varepsilon = \left(c_\mu^0\right)^{3+p/n} k^{3/2+m/n} \psi^{-1/n} \tag{2.14}$$

The shape of the equation (2.12) is suggested by the traditional model equations for ε, kl, and ω used in ocean modelling. By specifying appropriate values of the exponents p, m, n in (2.13), a number of well-known turbulence models can be directly recovered from this equation. Some examples are given in Table 2.1, including the standard Mellor–Yamada $(k - kl)$, $k - \varepsilon$ or $k - \omega$.

Table 2.1: Exponents p, n, m and relation to the variable of the second equation in some well-known two-equation models.

ψ	Two-equation model	p	m	n
kl	Mellor-Yamada (1982)	0.0	1.0	1.0
ε	Rodi (1987)	3.0	1.5	-1.0
ω	Wilcox (1988)	-1.0	0.5	-1.0

However, not all models fit perfectly well in the framework of the transport equation (2.13). For example, the model of Mellor and Yamada (1982) requires so-called wall functions to correctly reproduce the logarithmic part of the law of the wall and also differs slightly in the formulation of the turbulent transport terms.

2.2.2 Recovering Popular Two-equation Turbulence Models

2.2.2.1 Mellor-Yamada Model

The Mellor–Yamada level 2.5 model (Mellor and Yamada 1982) introduced in this section is one of a hierarchy of closures proposed by the authors in Mellor and Yamada (1974). This model has been applied to a wide variety of engineering and geophysical flows. The Mellor-Yamada level 2.5 model is recovered with Equations (2.9), (2.12) and (2.13) by specifying $p = 0.0$, $m = 1.0$ and $n = 1.0$ (see Table 2.1), as follow:

$$\frac{\partial k}{\partial t} + u\frac{\partial k}{\partial x} + v\frac{\partial k}{\partial y} + w\frac{\partial k}{\partial z} = \frac{\partial k}{\partial z}\left(\frac{A_v}{\sigma_k^{kl}}\frac{\partial k}{\partial z}\right) + P + B - \varepsilon \tag{2.15}$$

$$\frac{\partial kl}{\partial t} + u\frac{\partial kl}{\partial x} + v\frac{\partial kl}{\partial y} + w\frac{\partial kl}{\partial z} = \frac{\partial kl}{\partial z}\left(\frac{A_v}{\sigma_l}\frac{\partial kl}{\partial z}\right) + l\left(c_1 P + c_3 B - c_2 \varepsilon F_{wall}\right) \tag{2.16}$$

Where, σ_k^{kl} and σ_k are constant Schmidt number. In the standard implementation of the Mellor-Yamada model, $c_1 = 0.9$, $c_3 = 0.9$, $c_2 = 0.5$, and the wall proximity function is:

$$F_{wall} = 1 + E_2\left(\frac{l}{\kappa}\frac{d_s + d_b}{d_s d_b}\right)^2 \tag{2.17}$$

where $\kappa = 0.41$ is Von Karmans constant and $E_2 = 1.33$. The parameters d_s and d_b are the distances to the bottom and surface, respectively. The wall proximity function in Eq. (2.17) is the original parabolic shape suggested by Mellor and Yamada (1982). Other wall proximity functions can be also specified. For example, Blumberg et al. (1992) suggested a correction to the wall function for open channel flow, Burchard (2001) used another wall function for numerical experiments simulating an infinitely deep basin, etc.

2.2.2.2 $k - \varepsilon$ Model

The $k - \varepsilon$ model is one of the most common turbulence models, originally proposed by Jones and Launder (1972). The model was latter extended by Launder and Sharma (1974), Rodi (2017), etc., to take into account different complex situations including curvature, non isotropic turbulence, buoyancy effects and so on. The standard $k - \varepsilon$ model is based on the solution of the transport equation for the turbulent kinetic energy k and the transport equation for the dissipation rate ε. This model can be obtained with the generic length scale approach by specifying $p = 3.0$, $m = 1.5$ and $n = -1.0$ in Equations (2.9), (2.12) and (2.13) (see Table 2.1), which yields:

$$\frac{\partial k}{\partial t} + u\frac{\partial k}{\partial x} + v\frac{\partial k}{\partial y} + w\frac{\partial k}{\partial z} = \frac{\partial}{\partial z}\left(\frac{K_M}{\sigma_k^\varepsilon}\frac{\partial k}{\partial z}\right) + P + B - \varepsilon \tag{2.18}$$

$$\frac{\partial \varepsilon}{\partial t} + u\frac{\partial \varepsilon}{\partial x} + v\frac{\partial \varepsilon}{\partial y} + w\frac{\partial \varepsilon}{\partial z} = \frac{\partial}{\partial z}\left(\frac{K_M}{\sigma_\varepsilon}\frac{\partial \varepsilon}{\partial z}\right) + \frac{\varepsilon}{k}\left(c_{\varepsilon 1} P + c_{\varepsilon 3} B - c_{\varepsilon 2} \varepsilon\right) \tag{2.19}$$

where σ_k^ε is the Schmidt number for the eddy diffusivity of turbulent kinetic energy and σ_ε is the Schmidt number for the eddy diffusivity of dissipation. The model constants $c_{\varepsilon 1} = 1.44$, $c_{\varepsilon 2} = 1.92$ and $c_{\varepsilon 3}$ takes on one of two values depending on the sign of the buoyancy term (Burchard 2001).

2.2.2.3 $k - \omega$ Model

The $k - \omega$ model was originally created by Kolmogorov (1941). It is the first two-equation model of turbulence, which included one differential equation for k and a second for ω, defined as the rate of dissipation of energy per unit volume and time. The model were independently formulated later by (Saffman 1970), in which the parameter ω is considered as "a frequency characteristic of the turbulence decay process" and is related to dissipation by:

$$\omega = \frac{\varepsilon}{\left(c_\mu^0\right)^4 k} \tag{2.20}$$

Wilcox has continually refined and improved the model during the past three decades and demonstrated its accuracy for a wide range of turbulent flows Wilcox 1988; Wilcox 2008. The $k - \omega$ model can be obtained with the generic length scale approach by specifying $p = -1.0$, $m = 0.5$ and $n = -1.0$ in Equations (2.9), (2.12) and (2.13) (see Table 2.1), which yields:

$$\frac{\partial k}{\partial t} + u\frac{\partial k}{\partial x} + v\frac{\partial k}{\partial y} + w\frac{\partial k}{\partial z} = \frac{\partial}{\partial z}\left(\frac{K_M}{\sigma_k^\omega}\frac{\partial k}{\partial z}\right) + P + B - \varepsilon \tag{2.21}$$

$$\frac{\partial \omega}{\partial t} + u\frac{\partial \omega}{\partial x} + v\frac{\partial \omega}{\partial y} + w\frac{\partial \omega}{\partial z} = \frac{\partial}{\partial z}\left(\frac{K_M}{\sigma_\omega}\frac{\partial \omega}{\partial z}\right) + \frac{\omega}{k}\left(c_{\omega 1}P + c_\omega B - c_{\omega 2}\varepsilon\right) \tag{2.22}$$

where σ_k^ω is the Schmidt number for the eddy diffusivity of turbulent kinetic energy and σ_ω is the Schmidt number for the eddy diffusivity of dissipation. The model constant $c_{\omega 1} = 0.555$ and $c_{\omega 2} = 0.833$. and $c_{\omega 3}$ takes on one of two values depending on the sign of the buoyancy term (Burchard 2001).

2.2.3 Boundary Conditions

Boundary conditions are needed to solve the transport equations for turbulence quantities. In EFDC+, these conditions are set at the free surface and the bottom, involving velocities and tangential stresses. By specifying the kinematic shear stresses at the water surface and the bottom, the vertical boundary conditions for the turbulent kinetic energy and length scale equations are:

$$k_s = \frac{(u_*^s)^2}{\left(c_\mu^0\right)^2}, \quad k_b = \frac{(u_*^b)^2}{\left(c_\mu^0\right)^2} \tag{2.23}$$

where u_* is the friction velocity and the subscripts s and b refer to surface and bottom, respectively. The friction velocity vector u_* is calculated through the relation:

$$u_*^s = \sqrt{\frac{\tau_s}{\rho}}, \quad u_*^b = \sqrt{\frac{\tau_b}{\rho}} \tag{2.24}$$

where τ_s is the surface drag due to the wind, and τ_b is the bottom drag due to the friction.

Boundary conditions for the generic length-scale equation quantity ψ follow similar reasoning. The value of ψ is determined from (2.13), specifying $l = \kappa z$ and k from (2.23), yielding:

$$\psi_s = \left(c_\mu^0\right)^{p-2m} (u_*^s)^{m2} (\kappa z_s)^n, \tag{2.25}$$

$$\psi_b = \left(c_\mu^0\right)^{p-2m} (u_*^b)^{m2} (\kappa z_b)^n \tag{2.26}$$

where ψ_s, ψ_b are the surface and bottom values for ψ.

Chapter 3

EFDC+ GOTM Interface Implementation

3.1. General Concept

The general concept of the coupling EFDC+/GOTM is to transform 1D variables computed in GOTM into 3D fields used by EFDC+ and vice versa. For the implementation, a 1D profile of turbulence quantities, including turbulence kinetic energy, dissipation rate, macroscopic length scale, eddy viscosity, and eddy diffusivity, are calculated by GOTM. These quantities are then combined into 3D fields and used by EFDC+ subroutines. Some considerations must be taken into account for the solution's accuracy.

Firstly, the location of exchange variables in the grid cell must be consistent between the two codes. In GOTM, the discrete values for the mean flow quantities u, v, potential temperature Θ, and salinity S are located at the center of the intervals. In contrast, turbulent quantities like k, ε, and l are positioned at the interfaces of the intervals. However, variables and their derived parameters are located at the edge of the cells in EFDC+. Variables such as velocity components $u_{i,j}$, $v_{i,j}$ need to be converted to cell-centered quantities before being used by GOTM. To do that, a simple averaging can be used as:

$$u = 0.5\left(u_{i,j} + u_{i+1,j}\right) \tag{3.1}$$

$$v = 0.5\left(v_{i,j} + v_{i,j+1}\right) \tag{3.2}$$

where u and v are GOTM velocity components at the cell centre. $u_{i,j}$, $u_{i+1,j}$ and $v_{i,j}$, $v_{i+1,j}$ are EFDC velocity components at the edge of the cell.

Secondly, GOTM uses the potential temperature Θ as a variable in the heat transfer equation instead of the in-situ temperature T as in EFDC+. For an accurate estimation of the density and density gradients, the function `gsw_entropy_part` from `GSW Oceanographic Toolbox` of `TEOS-10` was adopted in the EFDC+ (McDougall and Barker 2011). During the simulation, this function calculates the potential temperature based on the general reference pressure and the temperature for each cell in the model domain.

Finally, GOTM is a one-dimensional model, only vertical diffusion of turbulence quantities is considered. In the current implementation of the coupling, the advective transport of the turbulent kinetic energy k and the turbulence dissipation rate ε are expanded through the utilization of the

advection-diffusion subroutine for constituents integrated within EFDC+. In order to reduce model run times, GOTM subroutines and variables are also refactored to use OpenMP multithreading technology.

3.2.   Coupling Implementation

To implement the coupling process, a module named `mod_gotm` has been added to the EFDC+ code. The module contains two subroutines, `init_GOTM` and `advance_GOTM`. The subroutine `init_GOTM` initializes all turbulence-related parameters by reading the `gotm_turb.jnp` input file and allocating memory for turbulence-related arrays. It also allocates memory necessary to perform solutions for a linear system of equations with a tridiagonal matrix using Gaussian elimination. The subroutine `advance_GOTM` serves as the module's core, where the turbulence module of GOTM is called. The turbulence is dynamically updated within this subroutine based on the specified turbulence closure model.

The algorithms of the subroutine `advance_GOTM` are described as follows. First, parameters including shear frequency squared `SS`, buoyancy frequency squared `NN`, surface and bottom friction velocities `GTAUS` and `GTAUB`, surface roughness `z0s` and the bottom roughness `z0b` are specified. The necessary parameters are transformed to suit a 1D water column model, i.e., 3D fields are transformed into a vertical vector. The transformed 3D fields are the layer heights `HPK` $\rightarrow$ `HPK1d`, the shear frequency squared `SS` $\rightarrow$ `SS1d`, the buoyancy frequency squared `NN` $\rightarrow$ `NN1d`, the turbulence kinetic energy `tke3d` $\rightarrow$ `tke1d`, the dissipation rate `eps3d` $\rightarrow$ `eps1d`, from which the integral length scale `GL1d` is calculated, the eddy viscosity `AV` $\rightarrow$ `num1d`, and the eddy diffusivity `AB` $\rightarrow$ `nuh1d`. The subroutine `do_turbulence` is called with the list of transformed arguments from the 3D model. It is noted that the list of arguments corresponds precisely to the mean flow and grid-related variables required to update the turbulent quantities. The subroutine `do_turbulence` is the central point of the turbulence module in GOTM. It determines the order in which turbulence variables are updated and calls other functions to update the 1D turbulence quantities. Finally, the 1D vertical vectors of turbulence quantities `tke1d`, `eps1d`, `num1d` and `nuh1d`, calculated by calling `do_turbulence`, are transformed back to original 3D fields in EFDC+. An extract of the code implementation for one cell of the 3D EFDC+ model is illustrated as follow:

```
! *** Set Up 1-D Arrays
HPK1d(1:NLAYER) = HPK(L,KSZ(L):KC) !< Layer thickness
num1d(1:NLAYER) = AV (L,KSZ(L):KC) !< Vertical turbulent eddy viscosity [m^2/s]
nuh1d(1:NLAYER) = AB (L,KSZ(L):KC) !< Vertical diffusion coefficient [m^2/s]
SS1d (0:NLAYER) = SS (L,KSZ(L)-1:KC) !< Shear Frequency Squared [1/s^2]
NN1d (0:NLAYER) = NN (L,KSZ(L)-1:KC) !< Buoyancy Frequency Squared [1/s^2]
tke1d(0:NLAYER) = tke3d(L,KSZ(L)-1:KC) !< Turbulent Kinetic Energy [m^2/s^2]
eps1d(0:NLAYER) = eps3d(L,KSZ(L)-1:KC) !< Turbulence Dissipation Rate [m^2/s^3]
GL1d (0:NLAYER) = GL3d (L,KSZ(L)-1:KC) !< Turbulence Length Scale [m]

! *** Update Turbulence Model
call do_turbulence(NLAYER, DELT, DEPTH, GTAUS, GTAUB, z0s_gotm, z0b_gotm, HPK1d,
NN1d, SS1d)

! *** Update 3D Fields of TKE, EPS, AV, AB
tke3d(L,KSZ(L)-1:KC) = tke1d(0:NLAYER)
eps3d(L,KSZ(L)-1:KC) = eps1d(0:NLAYER)
AV (L,KSZ(L):KC) = num1d(1:NLAYER) + AVOXY(L)
AB (L,KSZ(L):KC) = nuh1d(1:NLAYER) + AVBXY(L)
GL3d(L,KSZ(L):KC) = GL1d(1:NLAYER)
```

Chapter 4

EFDC+GOTM GUI and Input Requirements

4.1.   EFDC+ Explorer

The Graphical User Interface (GUI), EFDC_Explorer (EE) is a Microsoft Windows based pre-processor and post-processor for 3D EFDC+ hydrodynamic models developed by DSI, LLC (DSI). Development of EE has been ongoing since 1998.   Details of EE's options, features, as well as "User Manual" can be found from the website `"https://eemodelingsystem.atlassian.net/wiki/spaces/EK/overview"`.

4.2.   GUI for GOTM turbulence models

Following the implementation of EFDC+/GOTM interface, EE has been updated to support users building models with using turbulence closures from GOTM. A new option named `General Ocean Turbulence (GOTM)` has been added besides the original EFDC+ options in the `Vertical Turbulence Mixing` tab as shown in the Fig 4.1. Two methods are available to setup the turbulence models from GOTM.

The first method is recommended for users unfamiliar with GOTM. By simply dropdown the `Closure Model Presets`, users can switch between the options and select the desired one. EE will generate the input file with all the default parameters corresponding to the selected model. The options in `Closure Model Presets` include:

- Mellor - Yamada
- k - ε
- k - ω
- Generic
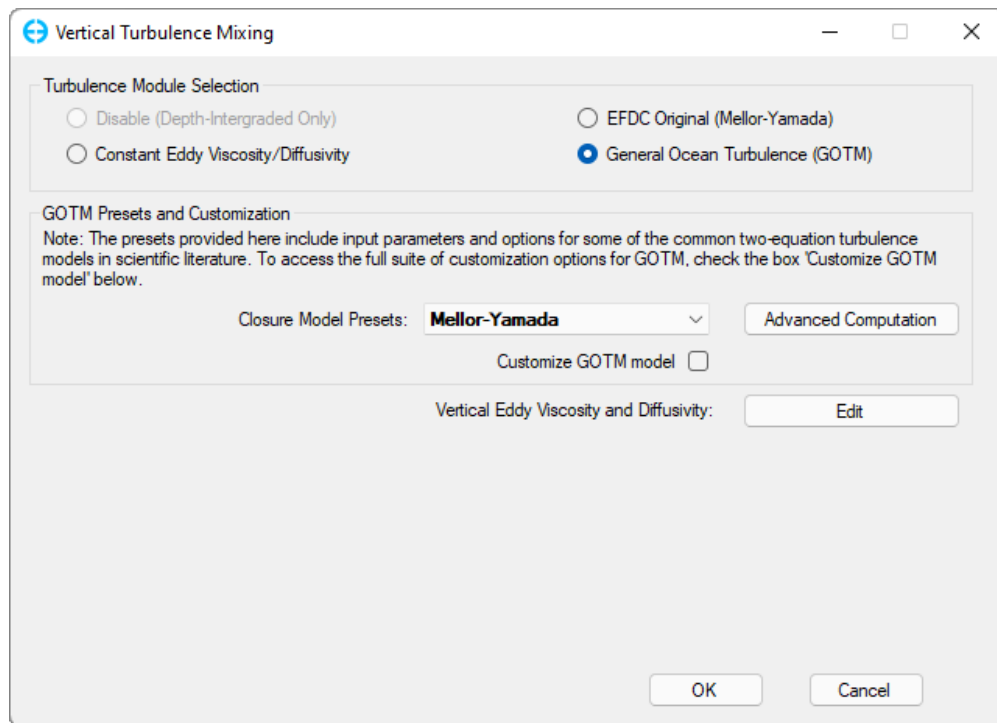
Figure 4.1: Vertical Turbulence Mixing Options.

The second method is more advanced that allow users to customize the turbulence model following the presetting base. By checking the box `Customize GOTM model`, the full suit of GOTM turbulence options will be displayed and ready to edit. The `Turbulence Closure` option includes `First-Order` and `Second-Order`. The `First-Order` method corresponds to models computing the diffusivities from the TKE and the turbulent length scale. TKE and length scale are computed from dynamic PDEs or algebraic relations. The `Second-Order` method is set by default, corresponds to a second-order model for the turbulent fluxes. The second-order models fall into different categories. As an essential part of GOTM, these models are discussed in detail in (ref GOTM document).

The `TKE equation` option specifies the appropriate routines for calculating the turbulent kinetic energy. The user has the choice between:

- Algebraic length scale equation
- Differential equation for tke (k-epsilon style)
- Differential equation for $q^2/2$ (Mellor-Yamada style)

On the `Length Scale Method`, the user has also the choice between several algebraic equations, and several differential transport equations for a length-scale determining variable, including:

- Algebraic length scale equation (e.g., parabolic, triangular, etc.)
- Dynamic dissipation rate equation

– Dynamic Mellor-Yamada q^2l equation

– Generic length scale (GLS)
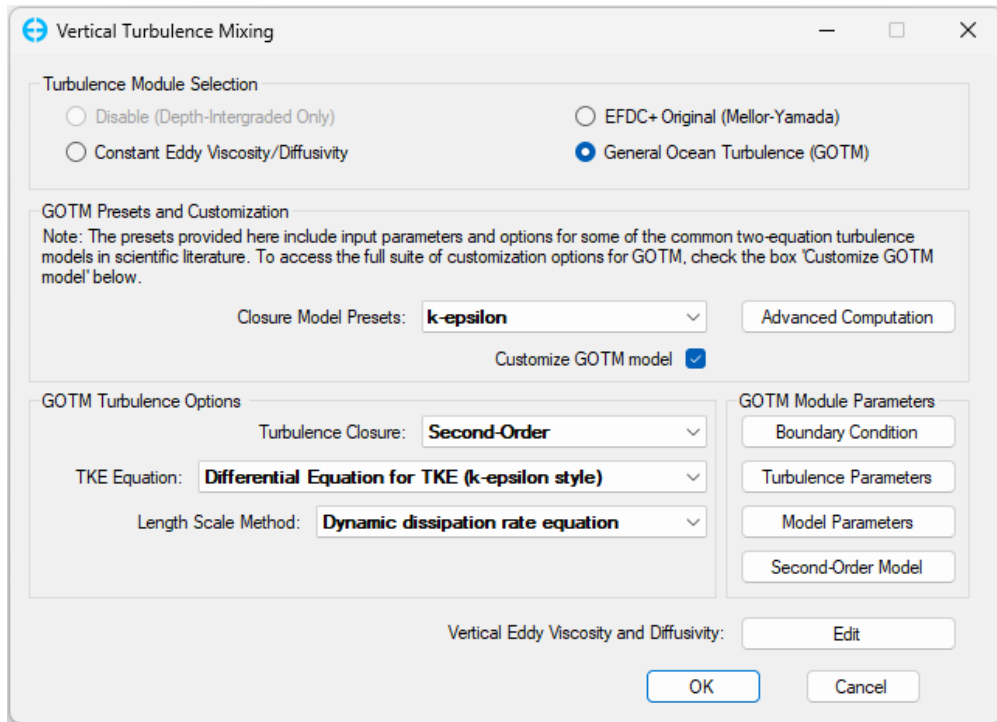
Figure 4.2: GOTM Turbulence Options.

Fig 4.2 illustrates an example of customizing setup of the k-epsilon model. The boundary conditions for `TKE equation` and `Length Scale Method` can be setup through `GOTM Boundary Conditions` tab (Fig. 4.3). The turbulence model parameters are given in the tabs `Turbulence Parameters`, `Model Parameters` and `Second-Order Model` as shown in Fig. 4.4, 4.5 and 4.6, respectively.
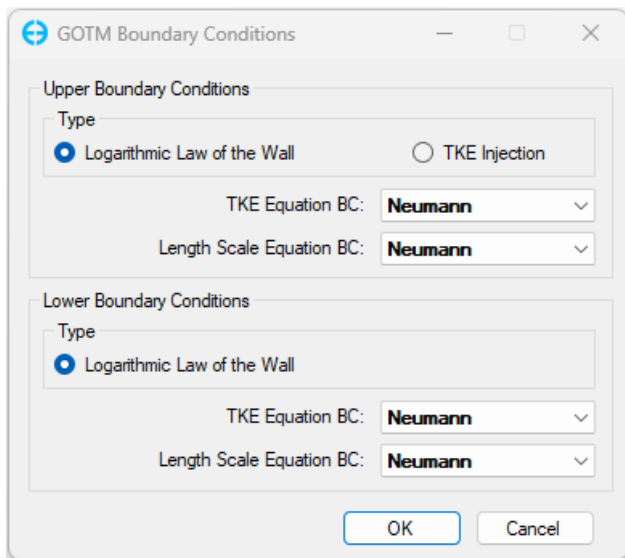
Figure 4.3: GOTM Boundary Conditions.
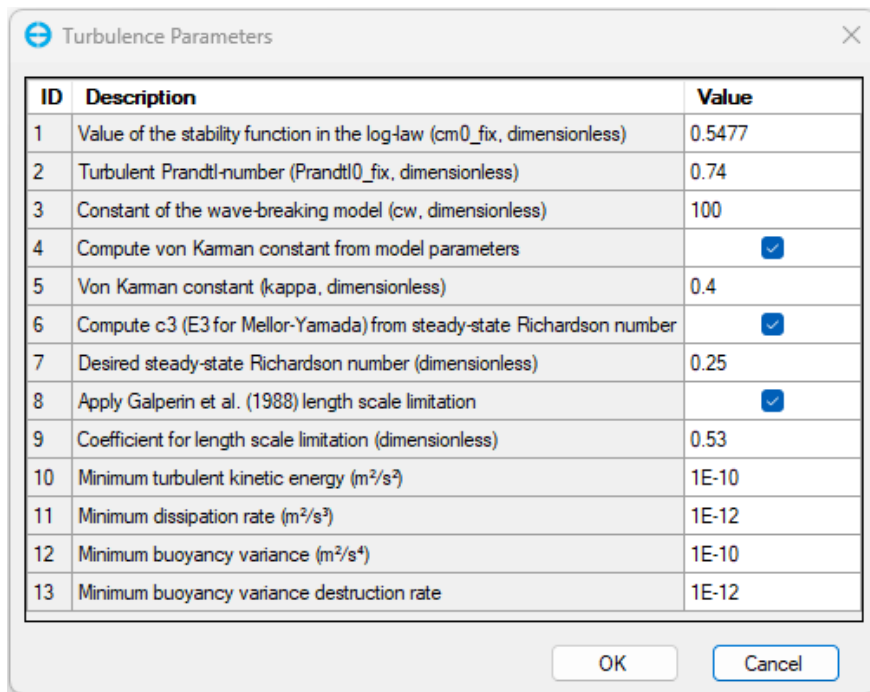
Figure 4.4: Turbulence Parameters.
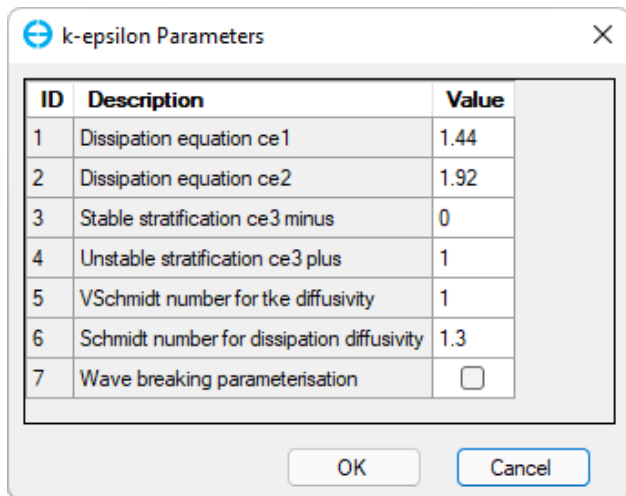
Figure 4.5: Model Parameters.
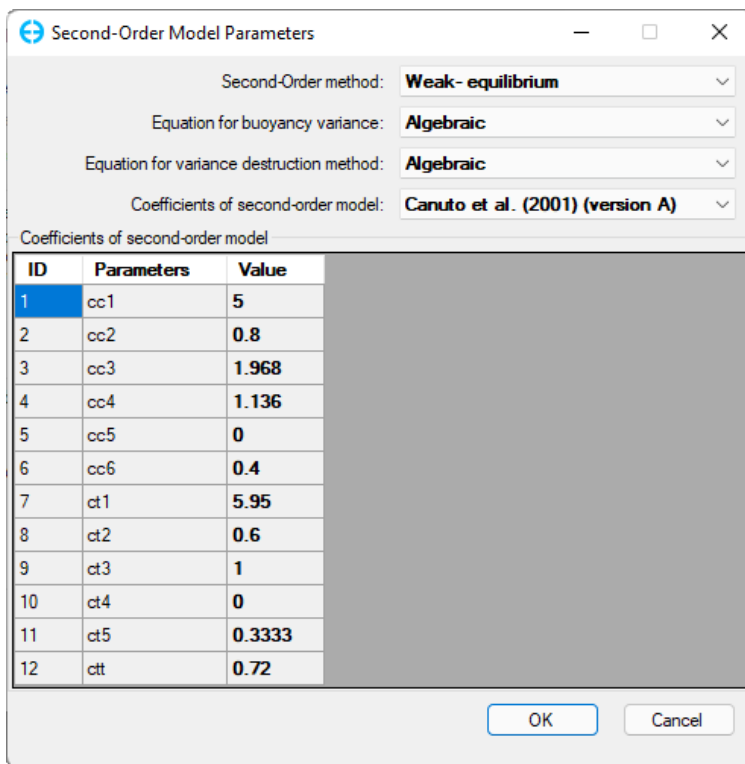
Figure 4.6: Second-Order Model.

4.3. Input file for GOTM turbulence models

Since EEMS version 10.2, DSI has taken advantages in applying JSON (JavaScript Object Notation) data format for EFDC+ input files. The format is easy to visualize the information and straightforward to add additional fields for new features. To avoid confusion with conventional JSON files, we have changed this new file extension in EFDC+ to JNP. JSON readers can still read and display this format. Some of the EFDC+ input files that use the new format include those related to MPI, propwash, and the new biota functionality. Following this enhancement, the input file for GOTM turbulence models also uses the JNP format. An extract of the `gotm_turb.jnp` file is illustrated as below:

```
"turbulence_method": 3,
"turbulent_kinetic_energy_eqn": 2,
"dissipative_length_scale": 8,
"stability_functions": 1,
"boundary_condition": {
   "upper_for_k_equation": 1,
   "lower_for_k_equation": 1,
   "upper_for_length_scale_equation": 1,
   "lower_for_length_scale_equation": 1,
   "upper_boundary_layer": 1,
   "lower_boundary_layer": 1
 }
```

Chapter 5

Case Studies

5.1. Open Channel Flow

Comparisons to steady uniform open-channel flows are useful for validation of more complicated hydrodynamic models because the characteristics of such flows can be computed analytically following Chow 1959, for example.

Following the example of Putzu et al. 2019, the velocity profile $U(z)$ can be computed as:

$$\frac{U(z)}{u_*} = \frac{1}{\kappa} \log\left(\frac{z}{z_r}\right) + C \tag{5.1}$$

where

u_* is the bottom friction velocity of the flow,

κ is the non-dimensional von Karman constant (0.4),

z is the vertical coordinate of depth,

z_r is the relative bottom roughness (Nikuradse),

C is a non-dimensional conductance coefficient determined to be 8.5 for the current example.

The eddy viscosity K_M can be computed analytically using a parabolic profile as:

$$K_M = \kappa u_* z \left(1 - \frac{z}{H}\right) \tag{5.2}$$

where H is the total flow depth, and all other variables are as defined previously.

For the present example, we specify the following parameters: $z_r = 0.03$ m; bed slope $i_f = 0.001$ m/m; friction velocity $u_* = 0.147$ m/s; and total flow $Q = 300 \ m^3/s$. These parameters result in a predicted mean velocity $\overline{U} = 2.47$ m/s, a uniform water depth $H = 2.428$ m, and a bottom shear stress of 21.713 N/m^2.

5.1.1 Description of the Test Case

The Open channel test-case here is based on the configuration described in Putzu et al. 2019 and Warner et al. 2005. Using the equations and specified parameters in the previous section, the velocity profile, shear stress, and eddy viscosity can be determined. The physical dimensions of the computational domain are specified as: Length, Width $L, W = 1000, 50$ m; Bed Slope $i_f = 0.001$ m/m; horizontal grid dimensions $dX, dY = 5, 5$ m; bottom roughness $z_0 = 0.001$ m; and vertical layers = 100.

The upstream model boundary conditions were specified using a flow boundary condition, whereby the total flow was distributed uniformly with depth. The downstream model boundary was configured using a specified water surface elevation (free tangential). To produce steady and reproducible results, the model was initialized with a uniform water surface elevation of 1 m. This resulted in an initial depth of 1 m at the upstream end of the computational domain, and 2 meters at the downstream end. The upstream flow boundary begins with an initial flow rate of 0 m^3/s and is gradually increased to the maximum discharge of 300 m^3/s at a rate of 0.1 m^3/s^2 over the course of 51 minutes. Simultaneously, the downstream boundary was initialized at 1 m above the model datum and gradually increased at a rate of 0.14 mm/s to reach the specified uniform water depth of 2.428 m 51 minutes after the start of the simulation.

Five different model configurations were tested with the open channel test-case: Mellor-Yamada (EFDC Original Approach); Mellor-Yamada (EEMS Preset for GOTM); $k - \varepsilon$ (EEMS Preset for GOTM); $k - \omega$ (EEMS Preset for GOTM); and Generic (EEMS Preset for GOTM).

All model configurations used the EFDC Legacy approach for bottom roughness, as described in Hamrick 1992. For all cases, horizontal eddy viscosity and diffusivity were neglected.

5.1.2 Results and Discussion

Comparison of the five model simulations with analytically-derived solution for the vertical profile of velocity is shown in Figure 5.1. All model simulations provide very close approximations to the logarithmic law of the wall within the log-law region of the flow. Within the log-law region, the velocity of the flow is largely related to roughness elements within the viscous sub-layer. Outside of the log-law region, all the model simulations show similar trends in the velocity profile, especially the two Mellor-Yamada closure options from EFDC+ origial and GOTM preset produced almost the same results. It is noted that for a reasonable comparison of the results, a correction to the wall function for open channel flow as proprosed by Blumberg et al. (1992) was used in for the Mellor-Yamada closure in both EFDC+ original and GOTM preset.
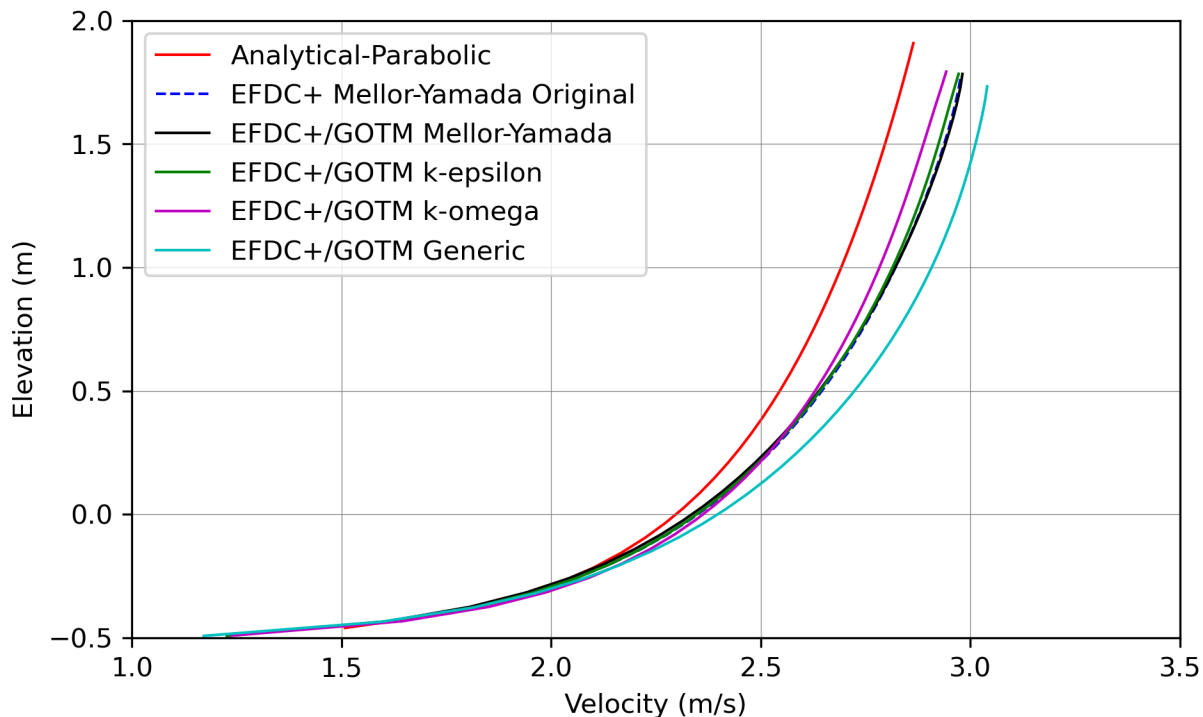
Figure 5.1: Comparison of the model-predicted velocity profile with the analytical law of the wall.

The vertical profile of eddy viscosity predicted by the different model configurations and the parabolic analytical solution are shown in Figure 5.2. Note that the parabolic eddy viscosity is based on the log-law velocity profile and is only valid in the log-law layer. Analytical models for flow velocity, depth, and eddy viscosity are two-dimensional and for uniform flows, while free-surface turbulent flows in river channels are strongly three-dimensional and non-uniform. Therefore, deviations are expected and reasonable when comparing a sophisticated three-dimensional model and analytical two-dimensional model. Regarding the model predictions, it can be noted that, similar to the velocity profiles, all models tend to predict very similar magnitudes of eddy viscosity over the depth profile.
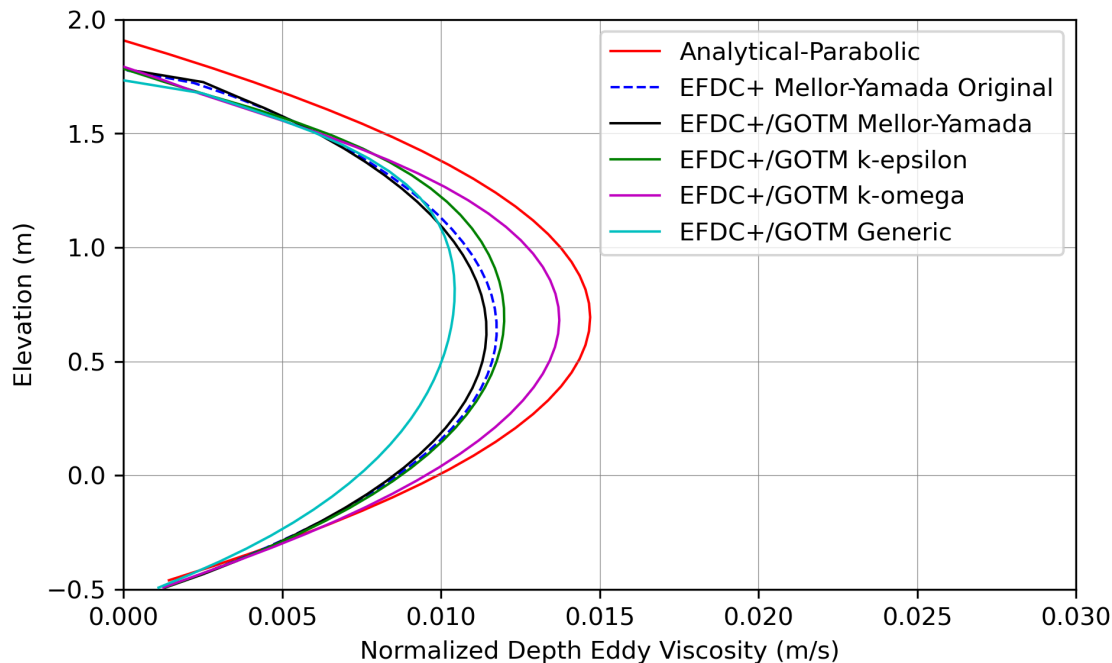
Figure 5.2: Comparison of the model-predicted eddy viscosity profile with the analytical parabolic approximation.

The vertical distribution of TKE within open channel flows reflects the balance between production and dissipation of TKE. In the open channel example, production to TKE is related to interactions with roughness elements within the viscous sub-layer. This leads to an approximately linear distribution as shown by Figure 5.3. It can be observed from Figure 5.3 that all parameterizations for turbulence closure considered in this example produce similar profiles.
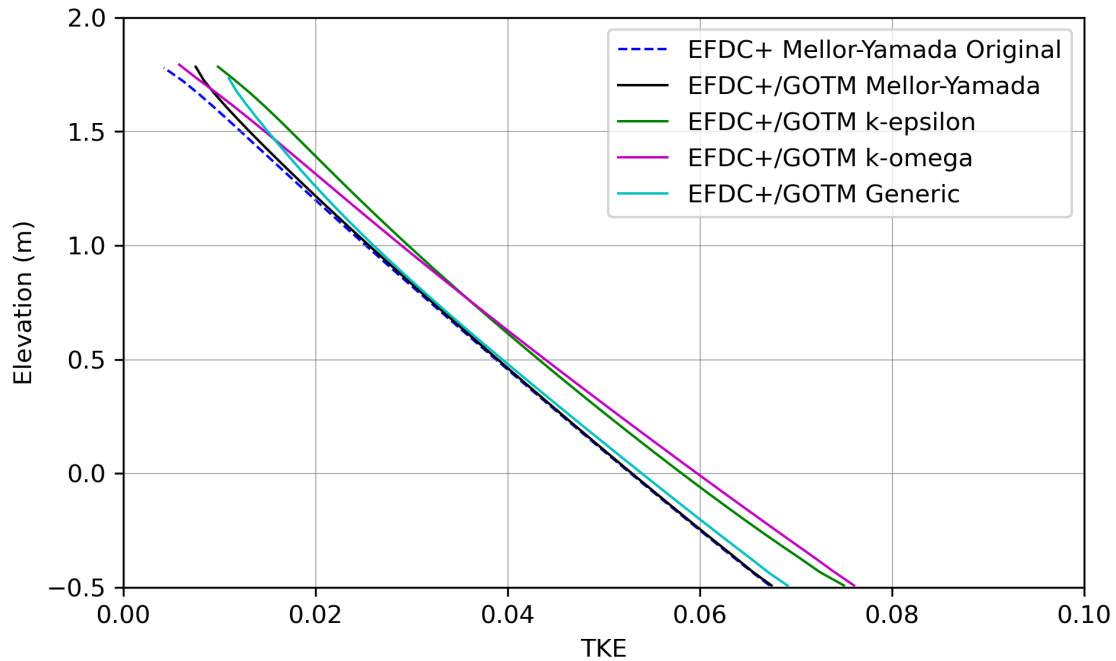
Figure 5.3: Comparison of model predicted turbulent kinetic energy profiles.

Table 5.1 provides a summary of the mean velocity ($\overline{U}$), flow depth (H), and bottom shear stress (τ_b) from the two-dimensional analytical solution and the five turbulence closure models tested in the open-channel flow example. It can be noted that most of the numerical model results are within 10% of the analytical model results. Both EFDC+ Mellor-Yamada (MY) and GOTM MY predictions were all within 5% of the analytical solution. The k-ε model predictions were well within 5% of the analytical solution for the mean velocity and the flow depth, the predicted bottom shear stress was within 5.9%. The k-ω and Generic closure models also produced reasonable values of mean velocity, depth, and bottom shear stress compared to the analytical solution.

Table 5.1: Statistical comparison of turbulence closure models and a two-dimensional analytical solution. The percent difference from the analytical solution is shown in parenthesis.

	Analytical	EFDC+ MY	GOTM MY	k-ε	k-ω	Generic
$\overline{U}$	2.47	2.58	2.57	2.57	2.56	2.56
[m/s]		(4.4%)	(4.0%)	(4.0%)	(3.6%)	(3.6%)
H	2.428	2.329	2.332	2.333	2.342	2.281
[m]		(-4.1%)	(-4.0%)	(-3.9%)	(-3.5%)	(-6.0%)
τ_b	21.713	20.623	20.682	22.993	23.313	21.196
$[\text{N/m}^2]$		(-5.0%)	(-4.7%)	(5.9%)	(7.4%)	(-2.4%)

5.1.3 Conclusion

The results of the five closure approaches, when compared to the two-dimensional analytical solution, demonstrated that each model produces comparable results. As an example of steady uniform open channel flow, subject only to the effects of viscosity and gravity relative to the inertial forces of the flow, this test case demonstrates that the coupling between EFDC+ and the GOTM subroutines was implemented properly. Additionally, these results demonstrate that each model can produce results which are physically realistic and comparable to simplified two-dimensional analytical approximations typical in the analysis of open channel flows.

5.2. Wind-driven entrainment in a rectangular flume

Momentum flux between the atmosphere and a water body is an essential driver of transport in estuaries, oceans, coastal environments, and lakes. The wind-induced mixing scenario evaluated here is similar to the experiments of Baines and Knapp (1965). The direct shear stress of the air flow on the water surface causes a surface movement that is steady in time. In a laterally enclosed body of water, the shear stress and surface current must give rise to an upward slope of the water surface in a downwind direction (Baines and Knapp 1965). For equilibrium, this slope produces a current in the upwind direction throughout the mass of water. This return current will not be evident near the surface because of the much stronger surface current (Baines and Knapp 1965, and Wu and Tsanis 1995). Flows related to wind-driven momentum transfer from the surface can be characterized by the surface and bottom friction velocity, u_{*s} and u_{*b} respectively (Wu and Tsanis 1995).

Analytical Profiles of Eddy Viscosity and Velocity

Wu and Tsanis 1995 described an analytical solution for these types of flows based on experiments in closed flumes under constant surface stress. A simple parabolic distribution of eddy viscosity can produce a close vertical profile in comparison to a sophisticated closure model (i.e., Mellor-Yamada or $k-\varepsilon$), and results in a double-logarithmic velocity distribution in the vertical. The eddy viscosity K_M distribution can be expressed as:

$$K_M = \left(\frac{\lambda u_{*s}}{H}\right)(z+z_b)(H-z+z_s) \tag{5.3}$$

where

u_{*s} is the surface shear velocity $\sqrt{\frac{\tau_s}{\rho}}$;

τ_s is the surface shear stress;

ρ is the density of water;

λ is a constant to characterize the intensity of turbulence;

H is the total water depth;

z is the vertical coordinate of depth;

z_b is the bottom roughness length scale; and

z_s is the surface roughness length scale.

For surface Reynolds numbers ranging from 10^3 to 10^5, λ varies from 0.2 to 0.5 and the average value is approximately 0.35. The velocity profile of Wu and Tsanis 1995 takes a double-logarithmic profile as:

$$U(z) = Au_{*s} \ln\left(1 + \frac{z}{z_s}\right) + Bu_{*s} \ln\left(1 - \frac{z}{z_b + H}\right) + C \tag{5.4}$$

where $U(z)$ is the horizontal velocity as a function of depth z. The following conditions are used to determine the coefficients A, B, and C: (1) At the free surface, the shear stress is evaluated by the wind velocity; (2) at the bottom, the velocity is equal to zero; and (3) the depth-averaged velocity (U) equals zero.

Using the non-dimensional variables $z_{sh} = \frac{z_s}{H}$ and $z_{bh} = \frac{z_b}{H}$, the foregoing three conditions are applied to (5.4) resulting in the values of coefficients A, B, and C:

$$A = \frac{q_2}{(p_1 q_2 - q_1 p_2)}; \tag{5.5}$$

$$B = -\frac{q_1}{(p_1 q_2 - q_1 p_2)}; \text{ and} \tag{5.6}$$

$$C = 0. \tag{5.7}$$

in which

$$p_1 = \lambda z_{sh}; \tag{5.8}$$

$$p_2 = \lambda \frac{z_{sh}}{z_{bh}}; \tag{5.9}$$

$$q_1 = (1 + z_{sh}) \ln\left(1 + \frac{1}{z_{sh}}\right) - 1; \text{ and} \tag{5.10}$$

$$q_2 = z_{sh} \ln\left(1 + \frac{1}{z_{bh}}\right) - 1. \tag{5.11}$$

Analytical Expressions for the Wind-Induced Setup and Seiche Period

Wu and Tsanis 1995 provide expressions for the wind-induced setup, which is a consequence of the water-gain region (leeward) and water-loss region (upwind), and can be used to confirm mass conservation in the simulation. Theoretically, the total setup $\Delta\zeta$ can be evaluated from the momentum equation as:

$$\Delta \zeta = \left(\frac{L}{gH}\right) u_{*s}^2 (1 - \eta) \tag{5.12}$$

where

L   is the length of the flume;

g   is the acceleration due to gravity ($9.81 \frac{m}{s^2}$); and

η is the ratio of the bottom to surface shear stress.

Due to the boundary effects of the closed flume, free gravity waves combine and form a standing wave, or seiche. The theoretical period of seiche T is calculated as:

$$T = \frac{2L}{\sqrt{gH}} \tag{5.13}$$

5.2.1   Description of the Test Case

Two EFDC+ test cases to were configured to represent the laboratory and analytical conditions described in Wu and Tsanis 1995 using two values of surface friction velocity (0.623, and 0.942 cm/s).

The physical dimensions of the model domain were specified as: Length, Width L, W = 5000, 100 m; horizontal grid dimensions dX, dY = 100, 100 m; total water depth H = 40 m; vertical layers = 100; surface roughness length = 0.0088 m; and bottom roughness length = 0.0056 m.

The model was configured with a constant surface friction velocity boundary condition of 0.623, and 0.942 cm/s. The effects of side-wall friction and horizontal eddy viscosity were not included in the simulation.

Five different model configurations were tested with the open channel test-case: Mellor-Yamada (EFDC Original Approach); Mellor-Yamada (EEMS Preset for GOTM); $k - \varepsilon$ (EEMS Preset for GOTM); $k - \omega$ (EEMS Preset for GOTM); and Generic (EEMS Preset for GOTM).

5.2.2   Results and Discussion

The results of the two scenarios provided are generally consistent with the mid-channel results of Putzu et al. 2019 trapezoidal basin case, as well as the simulation results of Wu and Tsanis 1995. A key point of deviation from the example of Wu and Tsanis 1995 was that the zero velocity condition at the bottom interface was not strictly enforced in the EFDC+ 3D model or the ROMS and Delft 3D models of Putzu et al. 2019. Note that in all cases, the bottom boundary condition for the 3D models (EFDC+, ROMS, and Delft 3D) corresponds to the top of the viscous sublayer, which is consistent with the law of the wall approximation rather than strictly enforcing the no-slip boundary condition (i.e., zero velocity). The different closure models tested in this example are compared below in terms of their vertical velocity profile at the mid-point of the channel, and in

terms of various statistics. In both cases, comparisons to the analytical solutions can be made, but the caveats above regarding explicit consideration of the no-slip boundary condition must be kept in mind.

Scenario 1: $u_{*s} = 0.623 \text{cm/s}$

The development of wind-induced velocity profiles in the closed rectangular flume necessarily result in zero net flow. Therefore, the depth-averaged velocity in all examples is zero. The deviations between closure models reflect the balance between production and dissipation of turbulent kinetic energy as parameterized by each model.

In Figure 5.4, it can be observed that the analytical solution, k-ε, k-ω, and Generic closure follow a similar profile from just below the surface to just above the bed (i.e., between approximately depths of 4 and 38 meters). Noted deviations occur at the surface and the bottom, as discussed previously with respect to the bottom velocity. Note that EFDC+ outputs the mean velocity for the cell (i.e., the average between the k and k + 1 face velocities), whereas the analytical model results are shown for each face velocities.
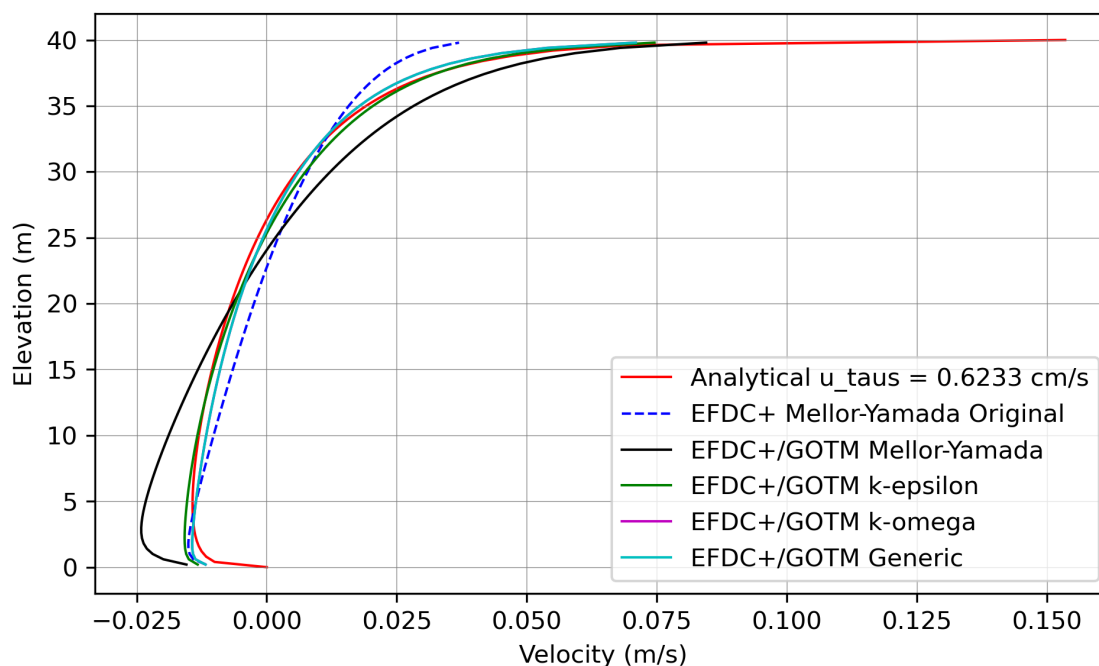
Figure 5.4: Velocity profile comparison between five closure model options and the analytical solution of Wu and Tsunis, 1995 for Scenario 1.

The most notable deviations from the analytical velocity profile come from the EFDC+ Original Mellor-Yamada and the EFDC+ Mellor-Yamada parameterization from GOTM. In the case of the Original Mellor-Yamada, the surface velocity was significantly under-estimated, while in the case of the GOTM-based Mellor-Yamada approach, the surface velocity was the highest of all closure

models evaluated, while the counter-current velocity near the bottom was larger in magnitude than all other closure models and the analytical model.

Table 5.2 presents statistical comparisons of the wind-induced setup, seiche period, zero velocity elevation, mean surface and bottom velocities with the analytical results. For Scenario 1, the different closure models evaluated showed small deviations in terms of the wind-induced setup, with all closure models under-estimating the analytical solution by 1-2%. The seiche period between the analytical model and all the closure models were identical (i.e., 0% difference). The zero velocity elevation reflects the elevation closest to the surface where the vertical velocity profile crosses zero. The k-ε, k-ω, and Generic closure models produced the most accurate predictions of the zero velocity elevation, with a percent under-estimation of between 3-4%. Both Mellor-Yamada closure models (i.e., EFDC+ Original and the GOTM approach) under-predicted the zero velocity elevation 2-4 meters or between 9-14%. All closure models under-estimated the analytically-derived surface velocity and over-predicted the analytical bottom velocity. As explained in relation to Figure 5.4, this is understandable to some extent because of the exact no-slip boundary condition enforced in the analytical model for the bottom velocity. Likewise, the surface velocity was systematically under-estimated due to the output of cell-centered velocities from EFDC+, compared to interface-based velocities from the analytical solution.

Table 5.2: Statistical comparison between five closure model options and the analytical solution of Wu and Tsunis, 1995 for Scenario 1. The percent difference between the analytical solution and each closure model is provided in parenthesis.

	Analytical	EFDC+ MY	GOTM MY	k-ε	k-ω	Generic
Wind-Induced Setup	4.95E-04	4.97E-04	4.88E-04	4.87E-04	4.89E-04	4.91E-04
[m]		(0%)	(-1%)	(-2%)	(-1%)	(-1%)
Seiche Period	504.8	505	505	505	505	505
[s]		(0%)	(0%)	(0%)	(0%)	(0%)
Zero Velocity Elevation	26.37	22.7568	24.0697	25.3499	25.6182	25.6068
[m]		(-14%)	(-9%)	(-4%)	(-3%)	(-3%)
Surface Velocity	11.11	3.68	8.44	7.45	7.09	8.01
[cm/s]		(-67%)	(-24%)	(-33%)	(-36%)	(-28%)
Bottom Velocity	-1.08	-1.41	-1.98	-1.45	-1.37	-1.55
[cm/s]		(31%)	(83%)	(34%)	(27%)	(44%)

Scenario 2: $u_{*s} = 0.942 \text{cm/s}$

Similar to the results of Scenario 1, Figure 5.5 demonstrates that the k-ε, k-ω, and Generic closure models produce very similar velocity profiles to the analytical solutions across the mid-depth range (i.e., from approximately 36 to 4 meters depth). As with Scenario 1, both Mellor-Yamada closure approaches deviated more significantly from the analytical model. The EFDC+ Original Mellor-Yamada approach significantly under-estimated the surface velocity, while the Mellor-Yamada approach implemented through GOTM predicted the highest surface velocity.

Table 5.3 provides statistical comparison between the analytical solution and the different closure
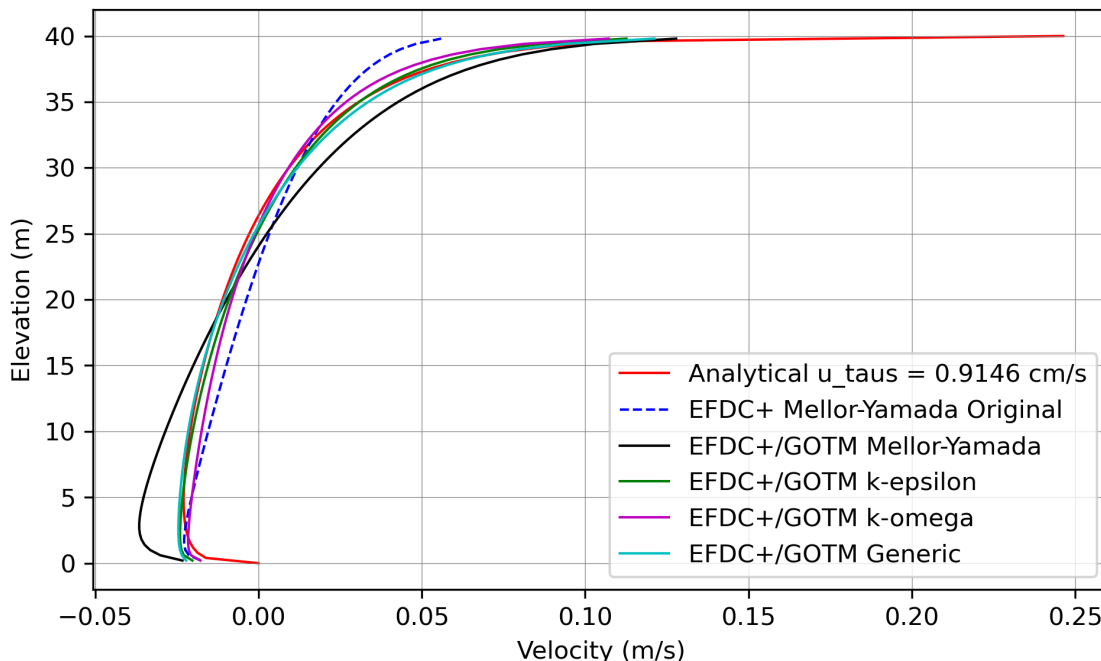
Figure 5.5: Velocity profile comparison between five closure models and the analytical solution of Wu and Tsunis, 1995 for Scenario 2.

models evaluated using EFDC+ and the EFDC+ GOTM interface. In the case of the wind-induced setup and seiche period, the Scenario 2 simulations produced numerical solutions identical to the analytical solution. The difference between the analytical solution and the numerical closure simulations for the zero velocity elevation was identical to Scenario 1, which was as expected given that the overall shape of vertical velocity profile did not change appreciably due to the increased surface friction velocity. The trends between Scenario 1 and 2 with regards to the surface and bottom mean velocities were also very similar, with all numerical turbulence closure models showing somewhat large but acceptable deviations compared to the analytical solution.

5.2.3   Conclusion

The results of the rectangular two-dimensional flume subject to wind-driven entrainment demonstrate that the numerical closure models were comparable to the analytical solution of Wu and Tsanis 1995. While deviations were especially apparent for the surface and bottom velocities, these differences were anticipated based on the differences in the parameterization of bottom and surface velocities between the analytical and numerical solutions. In comparing the numerical turbulence closure models evaluated in this example, the k-ε, k-ω, and Generic approaches provided comparable results which were generally superior to the Mellor-Yamada approaches. Of those three, the k-ω approach produced the results which were most consistent with the analytical solution.

Table 5.3: Statistical comparison between five closure model options and the analytical solution of Wu and Tsunis, 1995 for Scenario 2. The percent difference between the analytical solution and each closure model is provided in parenthesis.

	Analytical	EFDC+ MY	GOTM MY	k-ε	k-ω	Generic
Wind-Induced Setup	0.0011	0.0011	0.0011	0.0011	0.0011	0.0011
[m]		(0%)	(0%)	(0%)	(0%)	(0%)
Seiche Period	504.80	505.00	505.00	505.00	505.00	505.00
[s]		(0%)	(0%)	(0%)	(0%)	(0%)
Zero Velocity Elevation	26.37	22.73	24.05	25.27	25.62	25.61
[m]		(-14%)	(-9%)	(-4%)	(-3%)	(-3%)
Surface Velocity	16.78	5.59	12.78	11.26	10.71	12.12
[cm/s]		(-67%)	(-24%)	(-33%)	(-36%)	(-28%)
Bottom Velocity	-1.64	-2.13	-3.00	-2.28	-2.06	-2.34
[cm/s]		(30%)	(83%)	(39%)	(26%)	(43%)

5.3. Free Convection

Natural convection in a thermally stratified layer of water cooled from the free surface is a complex phenomenon because several energy transport processes must be taken into account simultaneously. Laboratory experiments are conducted to gain pertinent quantitative data for improved understanding of the detailed physical processes of buoyancy driven convective mixing in fluids cooled from the free surface. On the other hand, numerical models for predicting thermal characteristic are needed for real applications such as predicting vertical pollutant, nutrient and biota transport, etc in natural waterbodies (Behnia and Viskanta 1979).

Experimental evidence indicates that the vertical temperature structure near the air-water interface is usually composed of several regions depending on, in the case of natural waters, atmospheric conditions. The water surface temperature is almost always cooler than the water a millimeter below it (i.e., the cool-skin layer), except during intense insolation of quiescent water bodies (Behnia and Viskanta 1979).

Behnia and Viskanta (1979) introduced a simplified numerical solution for thickness of the convective mixed layer under constant surface heat flux:

$$h^2 = h_i^2 + 2\left(\frac{1+2\kappa}{\rho c \gamma}\right) \int_{t_i}^{t} H(0,\tau)\, d\tau \tag{5.14}$$

The dimensionless time τ is defined as:

$$\tau = \frac{\alpha t}{\delta^2} \tag{5.15}$$

where:

h is the convective (mixed) layer thickness;

i is the subscript indicating the initial time;

$H(0, \tau)$ is the (dimensionless) time variable total heat flux at the water surface ($z = 0$) taken as the sum of sensible, latent, and radiative energy fluxes;

κ is a proportionality factor that lies between zero and unity established from experimental data;

ρ is the density of water;

t is time;

α is the thermal diffusivity;

δ is the thickness of the surface skin layer;

c is the specific heat of water; and

γ is the temperature gradient.

Behnia and Viskanta (1979) demonstrated that mean values of κ between 0.25 and 0.35 provide a good fit to experimental data. For an experimental duration greater than 3 minutes, the numerical solution is insensitive to the value of κ, therefore the choice of a constant value is not a limitation to the range of applicability of this simplified model. Note that based on the comparison of the Behnia and Viskanta (1979) analytical solution to experimental data, both the degree of heat flux applied and the duration of the experiment result in the divergence of the analytical solution and experiment data in several instances. Therefore, we do not anticipate the numerical turbulence closure models to exactly reproduce the analytical solution. In general, because the analytical solution can both under- or over-predict the mixed layer depth experimental results, we expect some degree of convergence with the closure models evaluated for this example.

5.3.1 Description of the Test Case

The free convection test case is intended to demonstrate the development a surface mixed layer in a stably stratified fluid cooled from above. The scenario simulated here is similar to the numerical experiment of Van Roekel et al. (2018), the field study and numerical model of Large et al. (1994), and the laboratory experiment of Behnia and Viskanta (1979). The initial stratification was defined as a linear function with a surface temperature of 20º C and a bottom temperature of 18.5º C. The only forcing condition in the model was a constant negative surface heat flux of 75 Wm^{-2}.

The physical dimensions of the model domain were specified as: Length, Width L, W = 150, 150 m; horizontal grid dimensions dX, dY = 30, 30 m; total water depth H = 150 m; and vertical layers = 150. The effects of side-wall friction and horizontal eddy viscosity were not included in the simulation. Four different model configurations were tested with the open channel test-case: Mellor-Yamada (EFDC Original Approach); Mellor-Yamada (EEMS Preset for GOTM); $k - \varepsilon$ (EEMS Preset for GOTM); and $k - \omega$ (EEMS Preset for GOTM).

5.3.2   Results and Discussion

Compared to the analytical solution, all numerical models somewhat under-predicted the evolution of the mixed layer thickness by the end of the simulation (Figure 5.6). Based on the experimental data used by Behnia and Viskanta (1979), this may in some cases produce better results compared to experimental data than the analytical solution. Also, in comparing the numerical model results evaluated here to the numerical model results presented in Van Roekel et al. (2018) it can be observed that the results of that study also generally under-predicted the mixed layer thickness predicted by the analytical model, especially in the cases where a higher vertical grid resolution was applied. Nearly all of the numerical model configurations closely predicted the evolution of
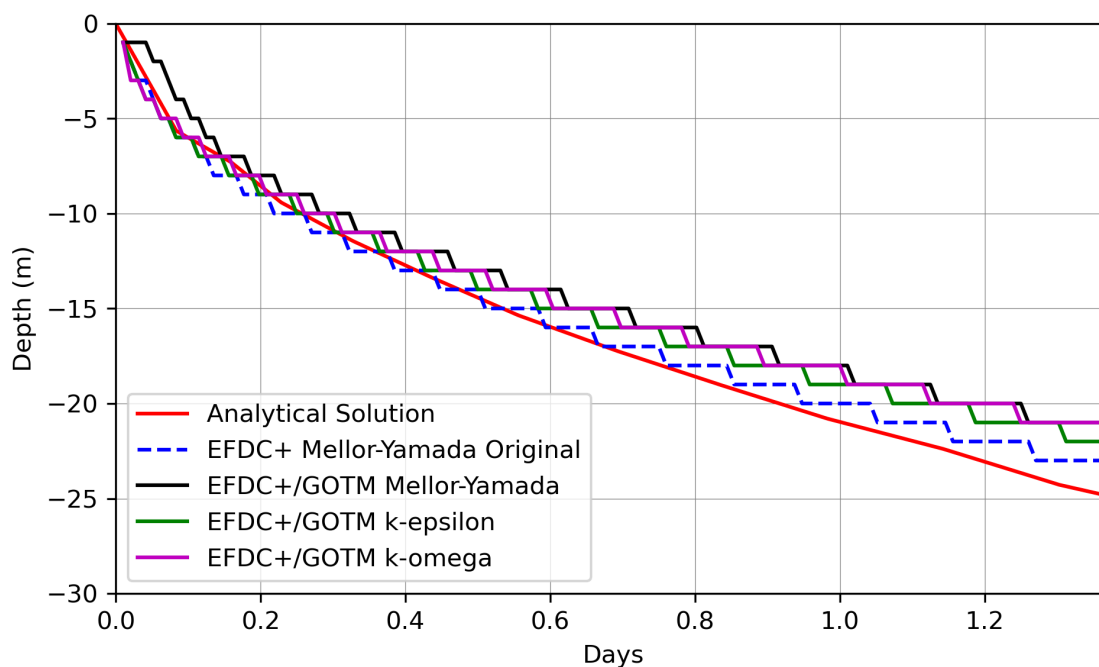
Figure 5.6: Mixed layer depth predicted by four numerical turbulence closure models and the analytical model of Behnia and Viskanta (1979).

the mixed layer depth shortly after initialization of the experiment. The only notable divergence from the analytical solution occured in the GOTM-based parameterization of the Mellor-Yamada approach at the beginning of the simulation. However, within about 5 hours from the start of the simulation, all of the numerical models generally converged with the analytical solution. All numerical model solutions tended to track with the analytical solution from 5 hours to 10 hours from the start of the simulation.

The pattern of the numerical model results with regards to the mixed layer depth shows a stair-step pattern in all cases. This was consistent with the numerical simulation of results of Van Roekel et al. (2018), and was a consequence of vertical discretization of the model. Essentially, once the gradient Richardson number becomes sufficiently large, successive layers of the model begin to mix rapidly. Therefore the pattern of the numerical model results reflect the point at which vertical mixing occurs between layers.

5.3.3 Conclusion

The results of the free convection test case demonstrated that all the numerical closure models evaluated for this example were capable of reasonably reproducing the predictions of the analytical solution. The EFDC+ Original Mellor-Yamada approach provided the closest fit to the analytical model.

5.4. Real application: Lake Washington model

5.4.1 Characteristics of Lake Washington

Lake Washington, situated adjacent to the city of Seattle, is the second largest natural lake in the State of Washington, and is one of the best examples in the world of a successful lake restoration by the diversion of sewage. The basin of Lake Washington (Figure 5.7) shows that it is deep, narrow, glacial trough with steeply sloping sides and deepest point approximately 65 m of depth. These morphologic features are highly suitable for application of the SGZ model. The lake has 35 km long and surface area of approximately 88 km^2. It is connected to Puget Sound via Lake Union and the Lake Washington Ship Canal, constructed in 1916. Mercer Island lies in the southern half of Lake Washington, separated from the lake's eastern shore by a relatively shallow and narrow channel, and from the western shore by a much wider and deeper channel.

The lake's two major influent streams are the Cedar River at the southern end and the Sammamish River at the northern end. The Cedar River contributes about 57 percent of the annual hydraulic load, while water from Lake Sammamish via the Sammamish River contributes 27 percent of the hydraulic load.

5.4.2 Model development

The computational domain comprises a horizontal curvilinear grid of 3185 cells, in which the range of grid size is from 100 to 200 m. The vertical direction is divided into 55 layers to provide sufficient discretization to investigate the effect of vertical density stratification due to vertical temperature gradients. Temperature with surface and bottom heat exchange are activated.

Boundary conditions are water discharge and temperatures at six inflow and one outflow boundaries. The two major inflow series located near the north and south regions of Lake Washington. The meteorological and atmospheric data such as wind speed, wind direction, relative humidity, air temperature and solar radiation were obtained from the King County web site and processed for the EFDC application. The initial temperature structure of Lake Washington was obtained from the Lake Washington buoy data. A water quality monitoring buoy, operated by King County Lake Monitoring Program (`https://green.kingcounty.gov/lake-buoy/default.aspx`), collects several vertical profiles each day for a range of constituents. The location of the buoy and other stations is shown on Figure 5.7.

The model runs for a period of one year from January 1st, 2010 through January 1st, 2011 to
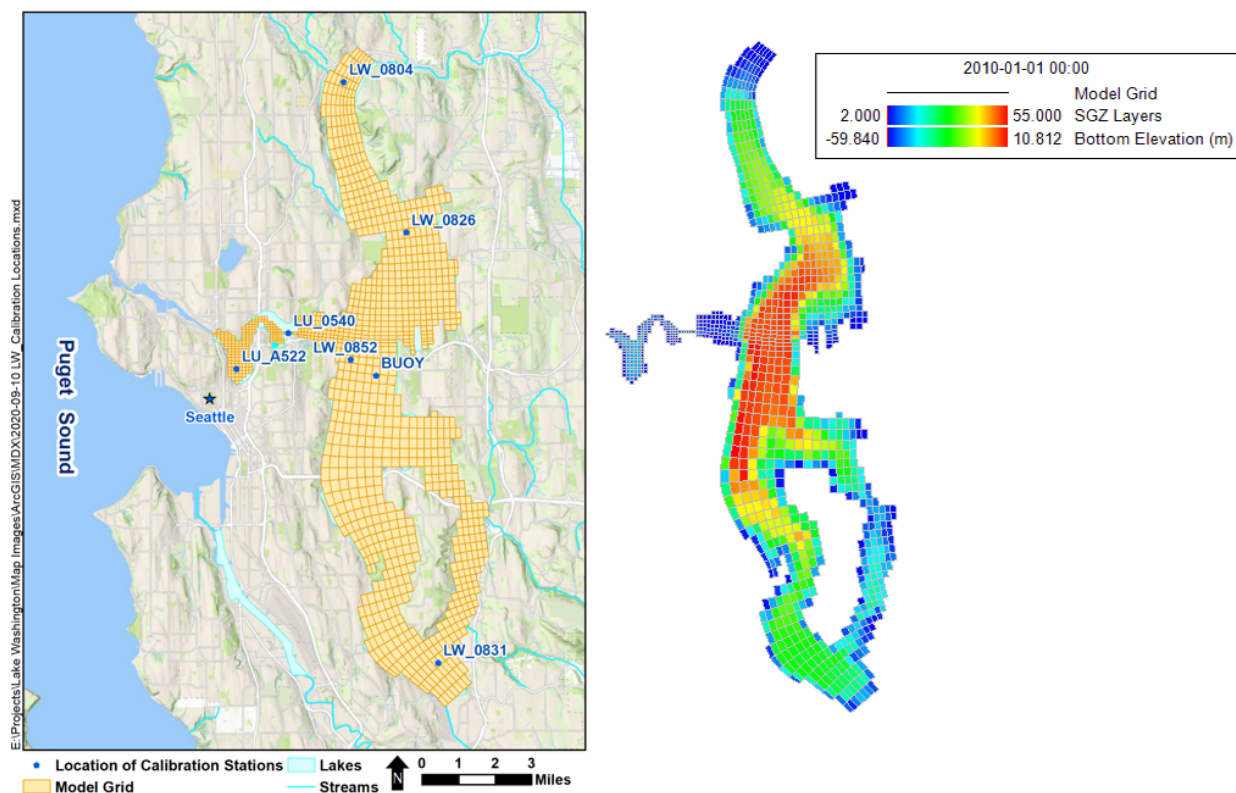
Figure 5.7: Lake Washington: Location of stations, Model grid, Bathymetry and number of layers for sigma-zed.

capture the annual cycle of thermal stratification. Four different model configurations were tested with the lake Washington model: Mellor-Yamada (EFDC Original Approach); Mellor-Yamada (GOTM Approach); $k - \varepsilon$ (GOTM Approach) ; $k - \omega$ (GOTM Approach).

All model configurations used the EFDC+ version 8.x approach for bottom roughness, as described in Hamrick (1992). For all cases, horizontal eddy viscosity and diffusivity were determined independently using Smagorinsky's subgrid scale closure formulation Smagorinsky (1963).

5.4.3   Results and Discussion

Figures 5.8 and 5.9 compare the observed and simulated water temperature at 10 m and 40 m of water depth at BUOY point. In general, the simulated water temperatures agree with observed data very well over the year. The model captured the major variance of water temperature both near the surface and the bottom of the lake. During the period of January to February, the water temperature is almost similar at the two depth levels. The difference of temperature at these levels started from Mars until the end of November and reach the peak for the period of August to September. This result reflects the annual cycle of stratification in the Lake Washington.

The annual cycle of thermal stratification representing one of the most important hydrodynamic processes occurring within the lake was also simulated. The Figure 5.10 shows a brief seasonal
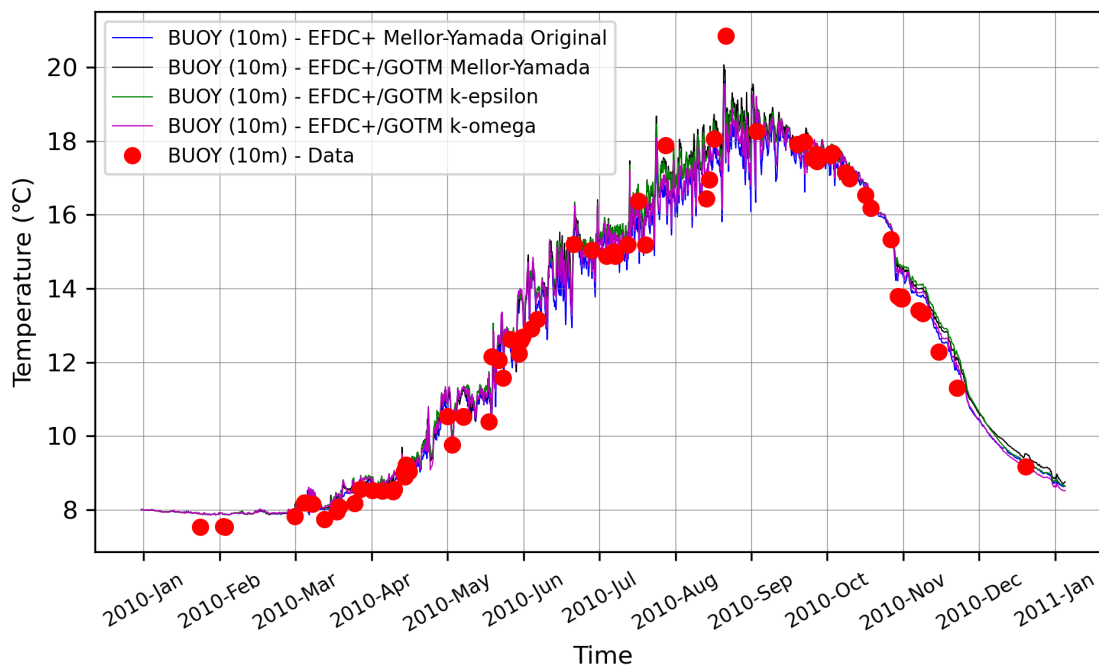
Figure 5.8: Temperatures at water depth 10m in Lake Washington. Comparison of the temperature time series produced by different turbulence models.
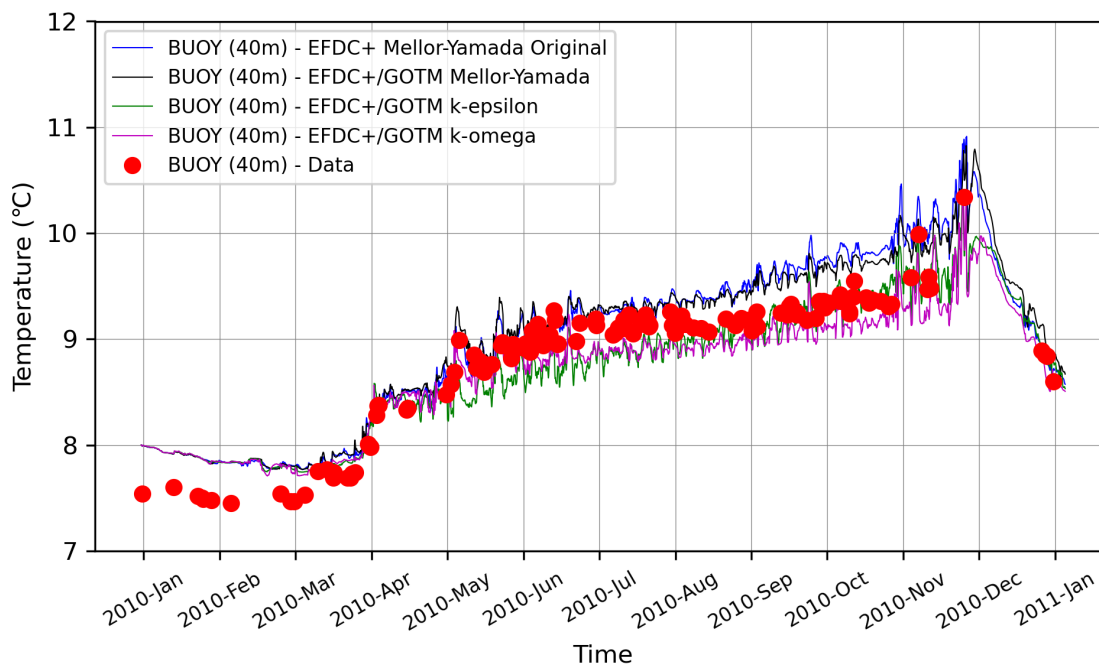
Figure 5.9: Temperatures at water depth 40m in Lake Washington. Comparison of the temperature time series produced by different turbulence models.

variation of vertical profile of the lake temperature at BUOY point reproduced by the numerical model with using the Mellor-Yamada turbulence closure, originally implemented in the EFDC+ code.
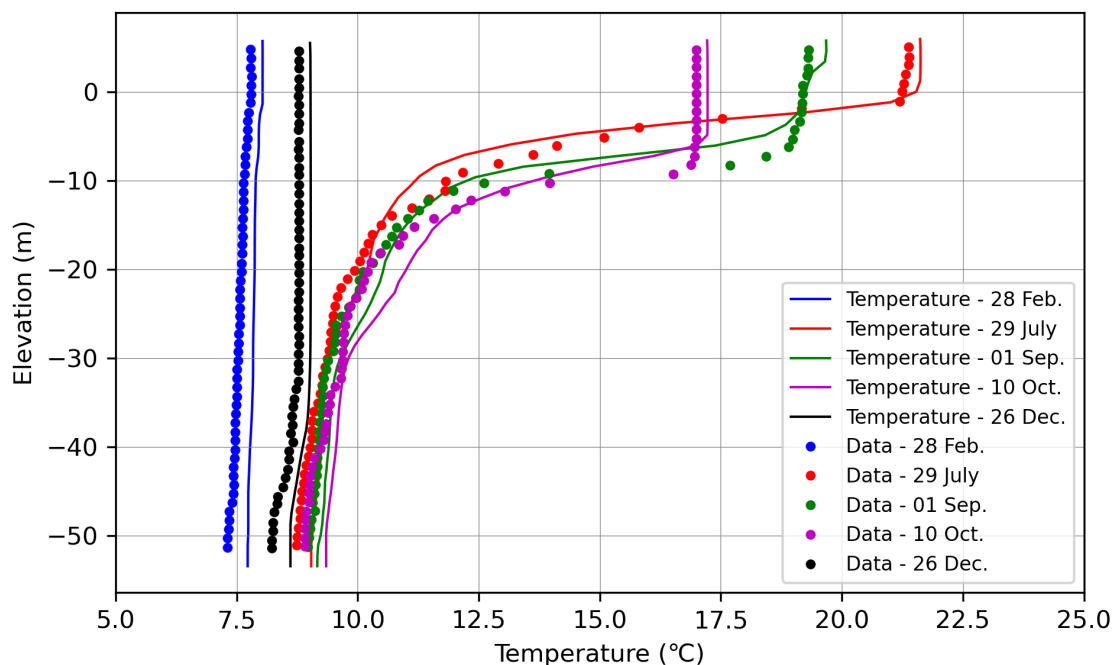
Figure 5.10: Comparison between model results and data of the water temperature vertical profile at BOUY point on several dates of the year (EFDC+ Original Mellor Yamada).

In the early spring (28 February), the temperature of the surface water was almost equal to that of the bottom water. Very little wind energy was needed to mix the lake completely, and the temperature of the lake became uniform near 7.5°C In the summer, the surface water continued to heat up due to the warm weather condition. The lake becomes stratified into three distinct zones: epilimnion, thermocline, and hypolimnion (in 29 July, 21.0°C on the surface and 9.0°C on the bottom). The rate of heat loss by evaporation and sensible heat then exceeds the radiation input, and the lake begins to cool in late summer (in 01 September, 18.5°C on the surface and 9.5°C on the bottom).

In the fall, the reductions of solar radiation and air temperature lead to cooling of the upper layers (in 10 October, 17.0°C on the surface and 9.5°C on the bottom). This cooling makes the surface water denser and causes mixing with deeper water, and the surface and bottom waters eventually approach the same temperature and density. This phenomenon, called "fall turn-over", was also reproduced by the numerical simulation.

The lake continues to lose heat to the atmosphere by evaporation and sensible heat, and the water temperature continues to decrease and the water column continues to be vertically mixed in the winter. As shown in 5.10, water temperature is almost uniform near 8.5°C in 26 December. The lake remains vertically mixed until the next spring, thus completing the annual stratification cycle.
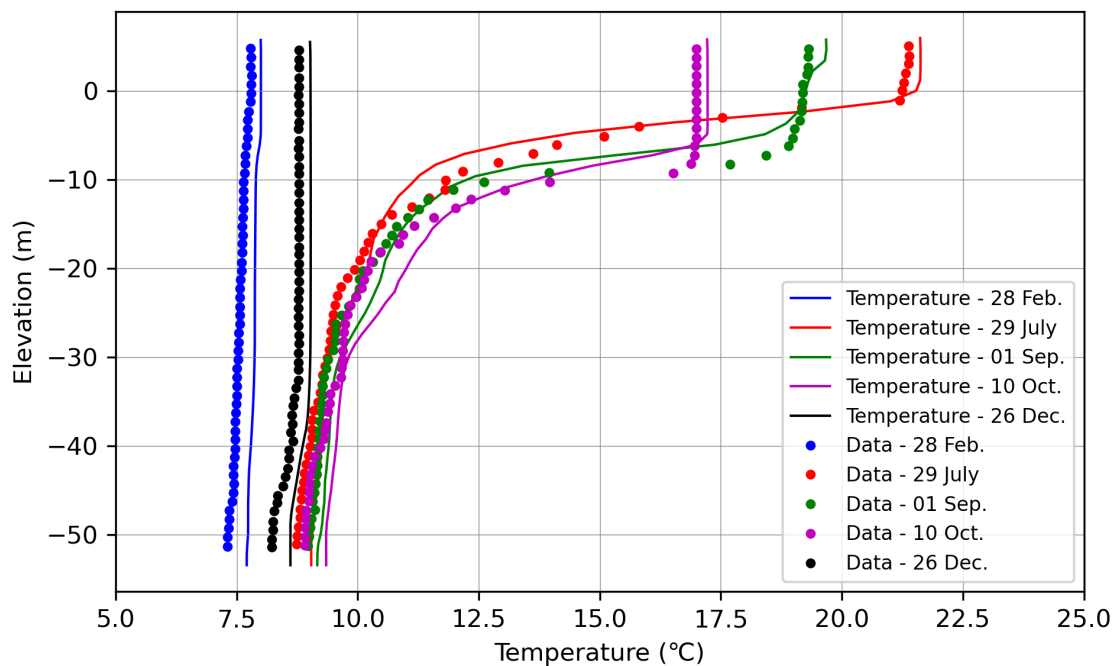
Figure 5.11: Comparison between model results and data of the water temperature vertical profile at BOUY point on several dates of the year (EFDC+/GOTM Mellor Yamada).
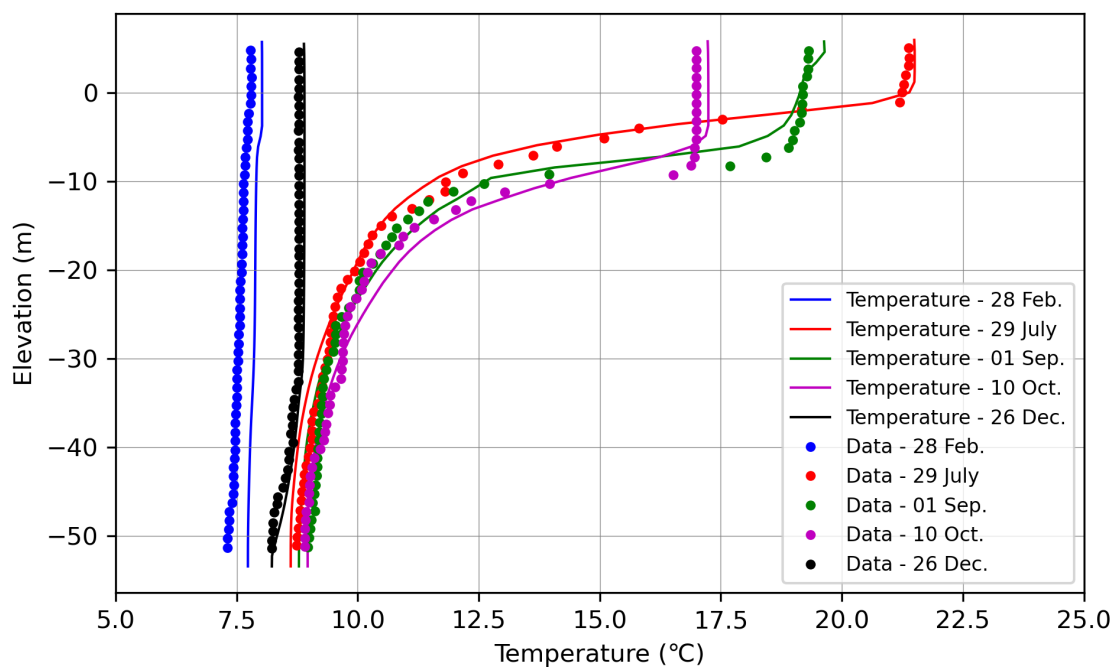
Figure 5.12: Comparison between model results and data of the water temperature vertical profile at BOUY point on several dates of the year (EFDC+/GOTM k-ε).

Similar results were also obtained with other turbulence closures from GOTM. Figures 5.11, 5.12 and 5.13 show the comparison between numerical simulation and observed data of the temperature vertical profile at BOUY point by using Mellor-Yamada (GOTM Approach); $k - \varepsilon$ (GOTM Approach) ; $k - \omega$ (GOTM Approach), respectively.
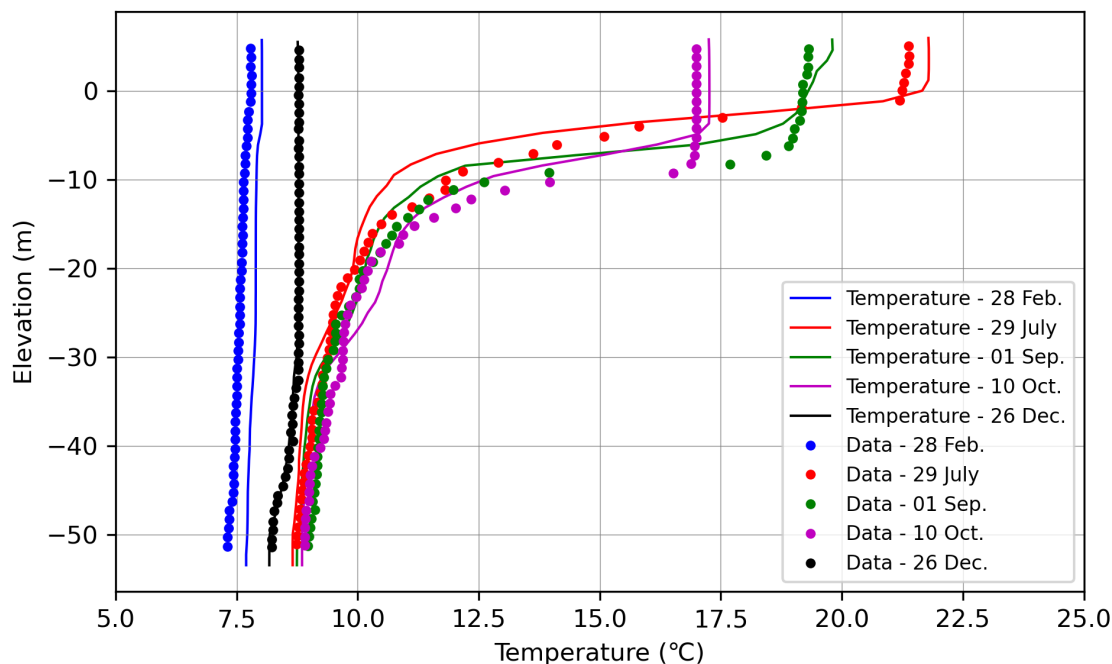
Figure 5.13: Comparison between model results and data of the water temperature vertical profile at BOUY point on several dates of the year (EFDC+/GOTM k-ω).

5.4.4 Conclusion

The results of the Lake Washington model demonstrated that all the turbulence closure models evaluated for this application were capable of reasonably reproducing the observed data. Even though the mixing depth was underestimated, the model heat transport and turbulence closure schemes behaved as expected with regard to water column stratification, turn-over and mixing.

Chapter 6

Conclusions

The EFDC+ code was coupled to the turbulence module of GOTM (which is a complete one-dimensional water column model) via the interfacing routine described in chapter 3. Along with that, the graphical interface EFDC_Explorer was updated to support users building models with using turbulence closures from GOTM described in chapter 4. With the aid of the GOTM, the turbulence models have shown the capability to represent vertical mixing in various situations.

The functioning of the coupled EFDC+/GOTM model was illustrated with four different test cases. These include three basic examples of open channel flow, the wind-driven entrainment in a rectangular flume, and free convection. The results of all test cases with different turbulence closure approaches, when compared to the analytical solution or observed data, demonstrated that each turbulence model produces comparable results. The capability of the EFDC+ model for a real-world application, different closure approaches have been compared with observed conditions of thermal stratification in Lake Washington (King County, Washington) model. Physical phenomenon with regard to water column stratification, turn-over and mixing have been accomplished. The results of these evaluations demonstrate that the coupling between EFDC+ and GOTM has been successfully implemented.

In addition, GOTM subroutines and variables were refactored to use OpenMP multithreading technology in order to improve the computational performance. Furthermore, it is also interesting to couple the EFDC+ code with the GOTM biological module, so-called GOTM-BIO in the same manner to the GOTM turbulence module. This module consists of seven state variables: phytoplankton, zooplankton, bacteria, particulate organic matter (detritus), dissolved organic matter and the nutrients nitrate and ammonium.

Chapter 7

References

[1] W. D. Baines and D. J. Knapp. "Wind Driven Water Currents". en. In: *Journal of the Hydraulics Division* 91.2 (Mar. 1965), pp. 205–221. ISSN: 0044-796X, 2690-2524. DOI: 10.1061/JYCEAJ.0001201. URL: https://ascelibrary.org/doi/10.1061/JYCEAJ.0001201 (visited on 11/02/2022).

[2] M. Behnia and R. Viskanta. "Free convection in thermally stratified water cooled from above". en. In: *International Journal of Heat and Mass Transfer* 22.4 (Apr. 1979), pp. 611–623. ISSN: 00179310. DOI: 10.1016/0017-9310(79)90064-4. URL: https://linkinghub.elsevier.com/retrieve/pii/0017931079900644 (visited on 11/02/2022).

[3] A. Blumberg, B. Galperin, and D. O'Connor. "Modeling Vertical Structure of Open-Channel Flows". In: *Journal of Hydraulic Engineering* 118 (Aug. 1992), pp. 1119–1134. DOI: 10.1061/(ASCE)0733-9429(1992)118:8(1119).

[4] H. Burchard. "On the q2l Equation by Mellor and Yamada (1982)". In: *Journal of Physical Oceanography - J PHYS OCEANOGR* 31 (May 2001), pp. 1377–1387. DOI: 10.1175/1520-0485(2001)031⟨1377:OTQLEB⟩2.0.CO;2.

[5] H. Burchard and K. Bolding. "Comparative Analysis of Four Second-Moment Turbulence Closure Models for the Oceanic Mixed Layer". In: *Journal of Physical Oceanography* 31.8 (2001), pp. 1943–1968. DOI: 10.1175/1520-0485(2001)031⟨1943:CAOFSM⟩2.0.CO;2.

[6] H. Burchard and K. Bolding. *GETM, A General Estuarine Transport Model: Scientific Documentation*. Tech. rep. Tech. Rep. EUR 20253 EN, Eur. Comm., Jan. 2002.

[7] H. Burchard, K. Bolding, and M. R. Villarreal. *GOTM, a general ocean turbulence model: theory, implementation and test cases*. Space Applications Institute, 1999.

[8] C. Chen, H. Liu, and R. C. Beardsley. "An Unstructured Grid, Finite-Volume, Three-Dimensional, Primitive Equations Ocean Model: Application to Coastal Ocean and Estuaries". In: *Journal of Atmospheric and Oceanic Technology* 20.1 (2003), pp. 159–186. DOI: 10.1175/1520-0426(2003)020⟨0159:AUGFVT⟩2.0.CO;2.

[9] V. T. Chow. *Open-channel hydraulics. Caldwell*. 1959.

References

[10] B. Galperin, L. Kantha, S. Hassid, and A. Rosati. "A Quasi-equilibrium Turbulent Energy Model for Geophysical Flows". In: *Journal of the Atmospheric Sciences* 45 (Jan. 1988), pp. 55–62. DOI: 10.1175/1520-0469(1988)045⟨0055:AQETEM⟩2.0.CO;2.

[11] D. B. Haidvogel, H. G. Arango, K. Hedstrom, A. Beckmann, P. Malanotte-Rizzoli, and A. F. Shchepetkin. "Model evaluation experiments in the North Atlantic Basin: simulations in nonlinear terrain-following coordinates". In: *Dynamics of Atmospheres and Oceans* 32.3 (2000), pp. 239–281. ISSN: 0377-0265. DOI: https://doi.org/10.1016/S0377-0265(00) 00049-X.

[12] J. M. Hamrick. *A three-dimensional environmental fluid dynamics computer code: Theoretical and computational aspects*. Tech. rep. Virginia Institute of Marine Science, College of William and Mary, 1992. DOI: https://doi.org/10.21220/V5TT6C.

[13] N. L. Jones and S. G. Monismith. "Modeling the influence of wave-enhanced turbulence in a shallow tide- and wind-driven water column". In: *Journal of Geophysical Research: Oceans* 113.C3 (2008). DOI: https://doi.org/10.1029/2007JC004246.

[14] W. P. Jones and B. E. Launder. "The prediction of laminarization with a two-equation model of turbulence". In: *International Journal of Heat and Mass Transfer* 15 (1972), pp. 301–314. URL: https://api.semanticscholar.org/CorpusID:121830285.

[15] A. N. Kolmogorov. "Equations of turbulent motion in an incompressible fluid". In: *Proceedings of the USSR Academy of Sciences* 30 (1941), pp. 299–303. URL: https://api. semanticscholar.org/CorpusID:118472206.

[16] W. G. Large, J. C. McWilliams, and S. C. Doney. "Oceanic vertical mixing: A review and a model with a nonlocal boundary layer parameterization". en. In: *Reviews of Geophysics* 32.4 (1994), p. 363. ISSN: 8755-1209. DOI: 10.1029/94RG01872. URL: http://doi.wiley. com/10.1029/94RG01872 (visited on 11/02/2022).

[17] B. Launder and B. Sharma. "Application of Energy Dissipation Model of Turbulence to the Calculation of Flow Near Spinning Disc". In: *Letters Heat Mass Transfer* 1 (Nov. 1974), pp. 131–137. DOI: 10.1016/0735-1933(74)90024-4.

[18] G. Madec, P. Delecluse, M. Crepon, and M. Chartier. "A Three-Dimensional Numerical Study of Deep-Water Formation in the Northwestern Mediterranean Sea". In: *Journal of Physical Oceanography* 21.9 (1991), pp. 1349–1371. DOI: 10.1175/1520-0485(1991) 021⟨1349:ATDNSO⟩2.0.CO;2.

[19] T. J. McDougall and P. M. Barker. "Getting started with TEOS-10 and the Gibbs Seawater (GSW) oceanographic toolbox". In: *Scor/Iapso WG* 127.532 (2011), pp. 1–28.

[20] G. L. Mellor and T. Yamada. "A Hierarchy of Turbulence Closure Models for Planetary Boundary Layers". In: *Journal of Atmospheric Sciences* 31.7 (1974), pp. 1791–1806. DOI: 10.1175/1520-0469(1974)031⟨1791:AHOTCM⟩2.0.CO;2.

[21] G. L. Mellor and T. Yamada. "Development of a turbulence closure model for geophysical fluid problems". In: *Reviews of Geophysics* 20.4 (1982), pp. 851–875.

References

[22] S. Putzu, F. Enrile, G. Besio, A. Cucco, L. Cutroneo, M. Capello, and A. Stocchino. "A Reasoned Comparison between Two Hydrodynamic Models: Delft3D-Flow and ROMS (Regional Oceanic Modelling System)". In: *Journal of Marine Science and Engineering* 7.12 (2019). ISSN: 2077-1312. DOI: 10.3390/jmse7120464. URL: https://www.mdpi.com/2077-1312/7/12/464.

[23] W. Rodi. *Turbulence models and their application in hydraulics: A state-of-the-art review, third edition*. Nov. 2017, pp. 1–108. ISBN: 9780203734896. DOI: 10.1201/9780203734896.

[24] P. G. Saffman. "A Model for Inhomogeneous Turbulent Flow". In: *Proceedings of the Royal Society of London. Series A, Mathematical and Physical Sciences* 317.1530 (1970), pp. 417–433. ISSN: 00804630. URL: http://www.jstor.org/stable/77591 (visited on 09/24/2023).

[25] J. Smagorinsky. "General circulation experiments with the primitive equations: I. The basic experiment". In: *Monthly weather review* 91.3 (1963), pp. 99–164.

[26] L. Umlauf and H. Burchard. "A generic length-scale equation for geophysical turbulence models". In: *Journal of Marine Research* 61 (Mar. 2003), pp. 235–265. DOI: 10.1357/002224003322005087.

[27] L. Umlauf and H. Burchard. "Second-order turbulence closure models for geophysical boundary layers. A review of recent work". In: *Continental Shelf Research* 25.7 (2005), pp. 795–827. ISSN: 0278-4343. DOI: https://doi.org/10.1016/j.csr.2004.08.004.

[28] L. Umlauf and H. Burchard. "Diapycnal Transport and Mixing Efficiency in Stratified Boundary Layers near Sloping Topography". In: *Journal of Physical Oceanography* 41.2 (2011), pp. 329–345. DOI: 10.1175/2010JPO4438.1.

[29] L. Van Roekel, A. J. Adcroft, G. Danabasoglu, S. M. Griffies, B. Kauffman, W. Large, M. Levy, B. G. Reichl, T. Ringler, and M. Schmidt. "The KPP Boundary Layer Scheme for the Ocean: Revisiting Its Formulation and Benchmarking One-Dimensional Simulations Relative to LES". en. In: *Journal of Advances in Modeling Earth Systems* 10.11 (Nov. 2018), pp. 2647–2685. ISSN: 1942-2466, 1942-2466. DOI: 10.1029/2018MS001336. URL: https://onlinelibrary.wiley.com/doi/10.1029/2018MS001336 (visited on 11/02/2022).

[30] J. C. Warner, C. R. Sherwood, H. G. Arango, and R. P. Signell. "Performance of four turbulence closure models implemented using a generic length scale method". In: *Ocean Modelling* 8.1-2 (2005), pp. 81–113.

[31] D. C. Wilcox. "Reassessment of the scale-determining equation for advanced turbulence models". In: *AIAA Journal* 26.11 (1988), pp. 1299–1310. DOI: 10.2514/3.10041.

[32] D. C. Wilcox. "Formulation of the k-w Turbulence Model Revisited". In: *AIAA Journal* 46.11 (2008), pp. 2823–2838. DOI: 10.2514/1.36541.

[33] J. Wu and I. K. Tsanis. "Numerical study of wind-induced water currents". In: *Journal of Hydraulic Engineering* 121.5 (1995), pp. 388–395.